Computational modelling of interaction effects in Fe_3O_4 nanoparticle systems for comparison with experiments

Ruţă Sergiu Ionel

Master of Science by Research

University of York
Physics

December 2013

Abstract

Fine particle magnetism is employed in a wide range of applications ranging from magnetic data recording to cancer therapies. Characterisation of nanoparticles is important for improving their applicability. This is a complex task, especially if magnetostatic interactions are to be considered. Here we have developed a methodology to investigate the inverse problem, which consists of extracting the magnetic properties such as anisotropy, size or saturation magnetisation from experimental magnetisation curves. For each set of magnetic properties a magnetisation curve can always be obtained, but from a magnetisation curve the parameters cannot always be uniquely determined. If interactions are significant the issue becomes complicated and the question of whether the parameters can be uniquely identified arises. To study this we simulated the magnetic behaviour of interacting nanoparticles with Monte-Carlo techniques and applied two different methods for studying the inverse problem. This allows to show that a unique extraction of model parameters is indeed possible only in a certain range of magnetic nanoparticle concentrations and temperatures. Using simulations we investigated the inverse problem for two parameters, anisotropy and saturation magnetisation, at different temperatures. At low temperature both parameters can be well determined, but the errors and the parameters correlation is dependent on the strength of the magnetostatic interaction. In the high temperature case, due to superparamagnetic behaviour, only the saturation magnetisation can obtain using the inverse problem approach. The methodology was also tested for a set of experimental measurements done on magnetite nanoparticles.

I would like to dedicate this thesis to my loving parents.

Contents

List of Figures

Acknowledgements

I would firstly like to thank Professor Roy Chantrell for the guidance, enthusiasm and encouragement during the last two years. I also want to thank Ondrej Hovorka for his patience, motivation, and continuous support of my research.

I would like to thank Sara Majetich and Ryan Booth for providing me the magnetic measurements. I thank my colleagues for the help and support they provided me, Joe Barker, Tom Ostler, Richard Evans, Unai Atxitia, Matthew Ellis, Ramon Cuadrado, Noi Chureemart.

Last but not least I would like to thank my family and friends for their friendship and support.

Declaration

In addition to the individual work of the author, this thesis contains the results of a collaboration with Proffessor Sara Majetich and coworkers at the Physics Department, Carnegie Mellon University, Pittsburgh, USA. The results consist of experimental measurements of magnetization curves and are used for applying the inverse problem methodology to experimental measurements. These results are presented in chapter 6.

All other work is the original work of the author except where explicitly indicated. This work has not been submitted to any other examining body or for any other qualification than the Degree of Master of Science at the University of York.

Ruţă Sergiu Ionel
York, December 2013

1

Introduction

Magnetic nanoparticles (NPs) are used in a broad spectrum of nanotechnologies. One of the most prominent examples is the magnetic information storage based on hard disk drives where NPs serve as basic memory blocks for storing the bits of information. In biology and chemistry functionalized magnetic NPs are widely used for detection of chemical species in solutions, inside cells, and biological fluids, where the noise patterns in their magnetisation response can be distinguished to serve similarly as colouring agents in the fluorescent detection. A very important use of NPs in medicine is as contrast agents in magnetic resonance imaging, which is a technique that allows monitoring diseases and organ functionality [1]. Magnetic NPs are also very promising for developing methodologies for cancer treatment where heat generated internally by NPs, when subject to high frequency external magnetic field sources, lead to a rapid destruction of a tumour [2][3]. Targeted drug delivery approaches where magnetic NPs act as carriers of drugs remotely navigated by external field gradients (magnetic forces) is another example of their application in biomedicine [1][2][3]. This list of applications is by no means exhaustive, which demonstrates importance of magnetic NPs in science and technology.

The above list of applications shares a range of challenges, which are crucial for their design and optimisation, and which will be in part addressed in this thesis. It is not trivial to manufacture magnetic nanoparticles of uniform shape, size, and identical physical parameters and so quantifying the properties of magnetic NP assemblies inevitably requires statistical description in term of probability distributions. Secondly, often magnetic NPs in applications are rather densely packed which leads to non-

negligible interparticle interactions. In the applications outlined above the interactions are mostly of magnetostatic or dipole-dipole character, as a result of their finite separation. Such interactions bring into play geometrical aspects when the arrangement of magnetic NPs considerably modifies the collective magnetic behaviour. Another complication is the temperature effect, which results in temperature dependence of physical parameters and in thermally activated dynamics. Superparamagnetic or hysteretic behaviour of the same system can be observed depending on the frequency of applied external magnetic fields. The main task in experiments is to try to predict based on a simple set of magnetization measurements the various distributions of properties, interactions, NP arrangement - such as clustering or packing fraction, and the intensity of thermal fluctuations.

To accomplish this task, magnetic characterisation of magnetic nanoparticle systems have been carried out by various means: FORC [4][5], $\Delta H(M,\Delta M)$-methods [6][7], fitting Langevin function to superparamagnetic curves[8]. The FORC method allows to calculate the interaction field and coercivity field distribution. The $\Delta H(M,\Delta M)$-methods are generally used to study the switching field distribution for perpendicular recording materials (the easy axis is aligned with the applied field direction). Roy Chantrell used the Langevin function to obtain the size and distribution of particles for superparamagnetic behaviour[8]. These approaches are based on a number of simplifications which limits their applicability. These techniques do not allow quantifying individual magnetic properties such as anisotropy, size and their distributions, in a general system (for example a system of random anisotropy vector distributions at any temperature).

In this thesis, we develop a general framework which allows interpreting magnetization measurements in terms of parameters of a realistic Monte-Carlo model of interacting system of magnetic NPs [9]. In the model, individual particles are described by the Stoner-Wohlfarth theory, which allows including distributions of particle volumes and random distributions of uniaxial anisotropy vectors common to realistic systems. Inter-particle interaction are modelled as dipole-dipole interactions, and the model allows incorporating various spatial arrangements of NPs. Thermal activation is included as well and the model allows capturing both superparamagnetic and hysteretic regimes. The model with its complexity is then combined with the least squares fitting tool based on the standard Levenberg-Marquard algorithm [10] into a unifying com-

putational tool, which allows a real time adjustment of parameters of the Monte-Carlo model to accurately describe (fit) input measurement data. The resulting output is a set of optimum model parameters which supposedly correspond to realistic properties of the experimentally investigated magnetic NP system.

In this way, the approach solves the inverse problem of identifying the model parameters from the measurement of magnetisation characteristics of NP systems. Inverse problems are generally difficult to deal with. Complete solution of an inverse problem requires in addition to obtain accurate description of input measurement data also answering the following questions:

1. Check the uniqueness of the solution. Is there just one set of values that describe the given data?

2. What are the errors in determining the solution?

If the uniqueness of the solution for the inverse problem is respected and the errors are small, then the method can be successfully applied to determine information such as saturation magnetization, anisotropy, particles size (mean value and distribution) or other parameters of interest.

For many applications, properties such as anisotropy (K) and saturation magnetization (M_s) are very important. For these reason the study done in this thesis is focused on these two parameters. The investigation is done for magnetite (Fe_3O_4) nanoparticles systems. K and M_s are strongly dependent on the size of particles and the method of preparation and coating[11]. For example, for magnetite nanoparticles M_s is decreasing with the size of the particle but also the coating affects the behaviour. For bulk magnetite material the saturation magnetization is 92 emu/g and the bulk value of uniaxial anisotropy of magnetite at 4K is $2.1 \cdot 10^5$ erg/cm^3 [12]. For magnetite nanoparticles the values are smaller, varying from 50 emu/g up to 90 emu/g. Coprecipitation preparation method give smaller values for M_s, whereas using thermal decomposition the values are closer to the bulk [13] [14][15][16]. Atomistic simulation confirms the finite size effect, but the values are larger than the experimental values [16]. The anisotropy of magnetite nanoparticles also vary in a large interval but different authors use different assumption in determining the value of anisotropy. Most of the values are determined from magnetization measurements using the coercivity field or the area of the hysteresis curve, or the blocking temperature. Other effect such as shape anisotropy

or dipole interaction can influence this type of calculation. In these case using simulation to solve the inverse problem is a good option to obtain quantitative information about K and M_s.

The thesis is structured as follows. In chapter 2 we briefly describe the main categories of magnetic materials. We focus on ferromagnetic materials and we describe the main contribution to the energy of a system of magnetic nanoparticles.

Chapter 3 contains the general theory of the Monte-Carlo model. We start with the Stoner-Wohlfarth model and we present the analytical description of it. Then the thermal effects are introduced and finally the Metropolis Monte-Carlo and kinetic Monte-Carlo algorithms are presented.

In Chapter 4 the numerical implementation of the algorithms are described. The implementation for simulating the magnetic behaviour of an interacting 3D system of spherical nanoparticles is presented in the first part of the chapter. The system contains particles with log-normal distribution of diameters and log-normal distribution of anisotropy values. Uni-axial anisotropy with random spherical distribution of easy axis is considered. The methodology for solving the inverse problem is presented in the second part of the chapter.

The validation of the algorithms is discussed in chapter 5. To test the Monte-Carlo model, results from simulations are compared with analytical calculations. Three different tests are made: reobtaining the Stoner-Wohlfarth model for low temperature limit, investigating coercivity as function of sweep rate and validating the combined kinetic Monte-Carlo and Metropolis Monte-Carlo algorithms in the superparamagnetic limit. At the end of the chapter the Levenberg-Marquardt and Grid Search methods presented in previous chapter are also tested.

Chapter 6 discusses, based on simulations, the uniqueness of the inverse problem for anisotropy and saturation magnetization. Then the methodology is applied for a set of experimental magnetization curves measured at different temperature.

2

Magnetic material. General overview

Magnetic properties of materials have as main sources the interaction between electrons with unpaired spins and the orbital motion of electron around the nucleus. The latter has a smaller contribution and in many cases is ignored [17]. There are three

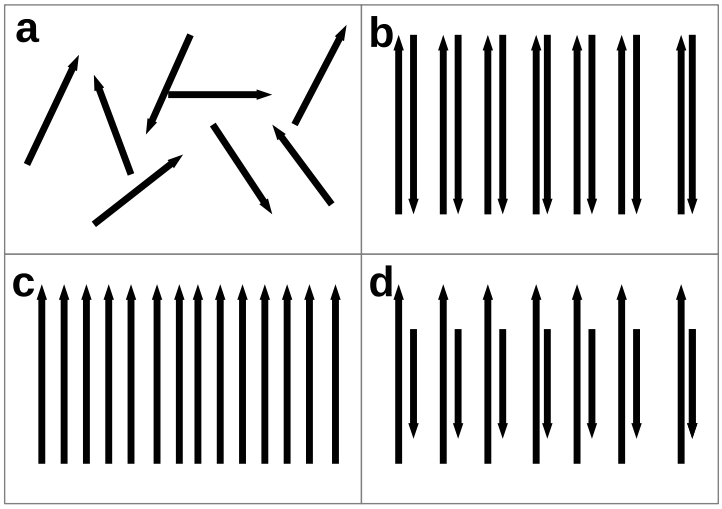

Figure 2.1: Types of magnetic materials. (a) paramagnetic: the unpaired spins of electrons are randomly oriented; (b) antiferromagnetic: the unpaired spins of electrons are anti-parallel oriented; (c) ferromagnetic: the unpaired spins of electrons are parallel oriented; (d) ferrimagnetic: the unpaired spins of electrons are anti-parallel oriented, but one orientation predominates.

main categories of magnetic behaviour (fig. 2.1):

1. paramagnetic: the unpaired spins of electrons are weakly coupled with each other and the spins are randomly oriented.

2. ferromagnetic: the unpaired spins of electrons strongly interact with each other and the spins are oriented parallel with each other.

3. antiferromagnetic: the unpaired spins of electrons strongly interacts with each other and the spins are oriented anti-parallel with each other.

There are also ferrimagnetic materials in which the the spins are anti-parallel coupled, but the number of spins pointing in one direction is larger than the spin pointing in the opposite direction. From a macroscopic point of view the behaviour is similar with ferromagnetic materials. Magnetite, which is investigated in this thesis, is a ferrimagnetic material.

To describe a magnetic material two main parameters are used: magnetization (M) and susceptibility. Magnetization is defined as the density of magnetic dipole moment per unit of volume. Susceptibility describes the variation of magnetisation with respect to an external magnetic field.

2.1 Ferromagnetism

The most common materials that exhibit ferromagnetic behaviour are iron, nickel and cobalt (Fe, Ni, Co). This types of materials have long range ordering. At the atomic level, unpaired spins align parallel with each other in a region called a domain. The magnetic field produced by one domain is large, but for a macroscopic sample the field is lower because the sample contains domains that are not necessary aligned. By decreasing the sample size there is a transition from multi-domain structure to a mono-domain structure. Brown investigated this transition and concluded that domain structures are formed to lower the total energy of the system and at certain size a mono-domain has lower energy than the multi-domain state.

In zero field and high temperature the total magnetic moment is zero due to the misalignment of domains. This behaviour is similar with paramagnetic materials and

is called superparamagnetism. In large fields the domains are aligned in the field direction. A maximum net magnetization is obtained. This value is called saturation magnetisation (M_s). A limitation of ferromagnets is represented by the Curie temperature. The saturation magnetisation of a material decreases with increasing temperature. At the Curie temperature there is a transition into a paramagnetic state, and the magnetic order disappears.

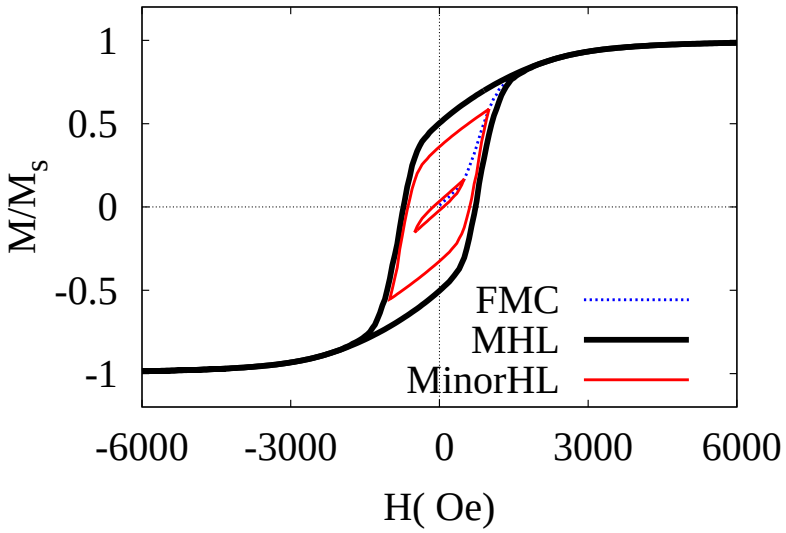

Figure 2.2: Types of magnetization curves. First Magnetization curve (FMC) is obtained by starting from a state with zero net magnetisation and increasing the applied field. Starting from a intermediary point on FMC and first decrease the field the Minor Hysteresis Loop (MinorHL) is obtained. The Major Hysteresis Loop (MHL) is obtained by starting from a relative large value of the net magnetisation.

Another aspect of ferromagnetic materials is the response to a magnetic field. A paramagnetic or a superparamagnetic material has zero magnetization if no external magnetic field is applied. If a large magnetic field is applied the magnetic moments align to the field direction and the material has a total magnetization, but if the field is removed the total magnetization is again zero. In the case of ferromagnetic materials, if a large magnetic field is applied and then reduced to zero, the total magnetization has a non zero value called remanence magnetisation (M_r). To decrease the magnetization to zero, a negative field (a field in the opposite direction) needs to be applied. If

the field is increased in the opposite direction even more, the magnetic moments will align to the field direction. If the field is decreased to zero and then increased in the opposite direction, the magnetization follows a similar behaviour. This variation of magnetization with respect to the applied field is called hysteresis. The current orientation of magnetic moment depends on the previous history. This is known as ”memory effect” and it is an important aspect for many applications such as magnetic recording. There are numerous types of magnetization curves as shown in figure 2.2: First Magnetization curve (FMC), Major Hysteresis Loop (MHL), Minor Hysteresis Loop (MinorHL), etc. In figure 2.3 a typical major hysteresis loop, usually referred as hysteresis loop or hysteresis curve, is illustrated. A hysteresis curve presents some characteristic elements:

1. Saturation magnetization (M_s), which is the magnetization value when all the moments are aligned with the field.

2. Remanence or remanence magnetization (M_r) is the magnetization value when a large external magnetic field is applied and then removed.

3. Coercivity field (H_c) is the magnetic field that needs to be applied so that the magnetization decreases from remanence value to zero.

For investigating magnetic properties of materials different techniques were developed covering different space and time scales such as first-principles calculation and atomistic models, micromagnetics based on LLG (Landau-Lifshitz-Gilbert) and LLB (Landau-Lifshitz-Bloch) equations and Monte-Carlo techniques. In these approaches the energy of the investigated system is studied. The main contributions to a system energy are determined by internal factors such as anisotropy energy, inter-particle interaction or external factors such as an external magnetic field. The inter-particle interaction can emerge from quantum effect (exchange interaction, Kondo interaction, Dzyaloshinskii-Moriya interaction) or can be magnetostatic in origin. The first type of interaction is short range and this thesis is focused on nanoparticle system where this interaction can be neglected. It is assumed that the nanoparticles are separated by a surfactant. This removes the possibility of exchange coupling, leaving magnetostatic effect as the dominant interaction. Next, the main contribution to the investigated sys-

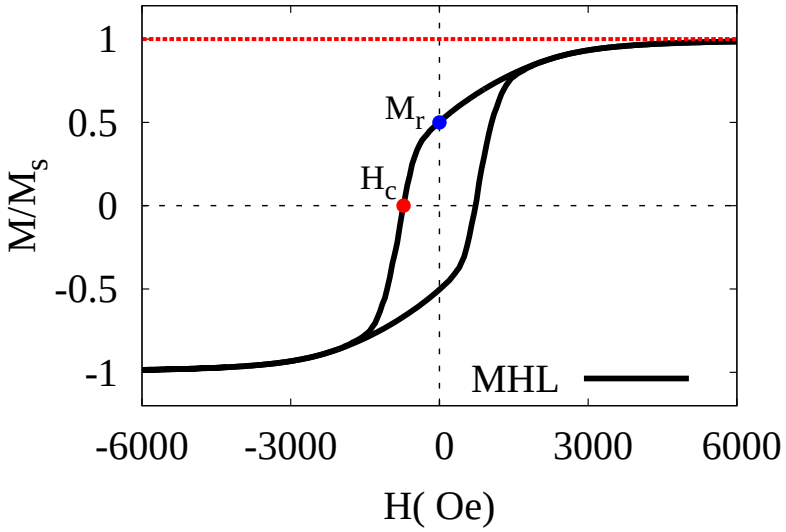

Figure 2.3: Major hysteresis loop. If a large magnetic field is applied and then reduced to zero, the total magnetization has a non zero value called remanence magnetisation (M_r). To decrease the magnetization to zero, a negative field (a field in the opposite direction) needs to be applied (H_c).

tem energy are described: Zeeman energy, magnetostatic energy and different type of anisotropy energies.

2.2 Zeeman energy

For the investigation of hysteresis curves the contribution of external field to the system energy must be included. The energy of a particle in an external magnetic field is called Zeeman energy and is defined by the following relation:

$$E_Z = -\mu_0 M_s V \vec{e_M} \cdot \vec{H_{ap}} \tag{2.1}$$

where μ_0 is the permeability of free space. In cgs (centimetre–gram–second system) μ_0 is 1 and in SI (International System of Units) μ_0 is equal to $4\pi 10^{-7}$ H/m. V is particle volume and H_{ap} is the applied field. $\vec{e_M}$ is the versor of the magnetisation vector.

2.3 Magnetostatic energy

In system of closed packed particles dipole-dipole interaction plays an important role in the system behaviour. If the system is very diluted the dipole interaction is small and can be neglected, but if the particles are arrange closer to each other the dipole field contribution to the total energy increases and becomes important. For a sample of magnetic particles the standard way to compute the dipole field created by all the particles acting on a particle i is given by following equation[18]:

$$\vec{H}_i = \sum_{\substack{j \\ j \neq i}} \frac{M_s V}{4\pi\mu_0 r_{ij}^3} \left[\frac{3}{r_{ij}^2} (\vec{e_{Mj}} \cdot \vec{r_{ij}}) \vec{r_{ij}} - \vec{e_{Mj}} \right] \tag{2.2}$$

The corresponding energy term can be written exactly the same as the Zeeman energy with the interaction field H_i instead of the applied field H_{ap}.

2.4 Anisotropy energy

Magnetic properties of different materials are in general dependent on the direction of the measurement. In the absence of a external magnetic field the magnetic moment will orient itself on one or more preferential directions. These directions are called easy axes. To include this effect, the total energy contains one term that depends on the direction of magnetic moments. This term is known as anisotropy energy. The anisotropy energy density takes values in a large domain from approximately 0.005 MJ/m^3 ($5 \cdot 10^4$ erg/cm^3) up to 10 MJ/m^3 ($1 \cdot 10^8$ erg/cm^3) [19]. There are different sources of anisotropy: magnetocrystalline anisotropy, shape anisotropy, stress anisotropy, exchange anisotropy. For an isotropic material the energy distribution is a sphere. Depending of the anisotropy complexity the symmetry of energy distribution is reduced, as it can be seen in figure 2.4 for uniaxial anisotropy and in figure 2.5 for cubic anisotropy.

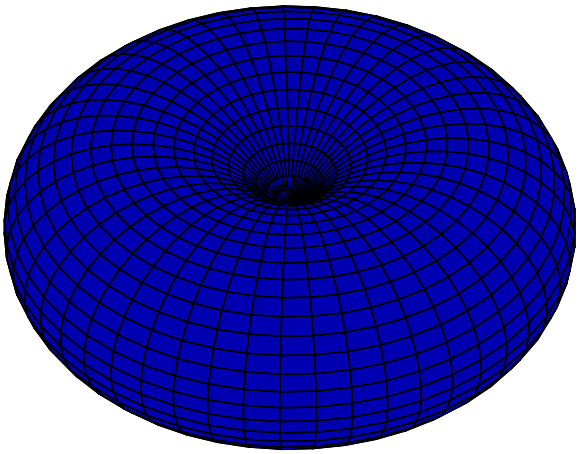

Figure 2.4: Energy distribution for uniaxial anisotropy: $K_1 > 0$ and $K_2 = 0$.

2.4.1 Magnetocrystalline anisotropy

The main source of magnetocrystalline anisotropy is the indirect interaction of the spin with the crystallographic lattice mediated by spin-orbit coupling and orbit-lattice coupling. The magnetostatic energy is described mathematically based on phenomenological approaches as a series expansion depending on the crystal structure symmetry [19]. In general two types of magnetocrystalline anisotropy are considered uniaxial anisotropy and cubic anisotropy. If a magnetic material with uniaxial anisotropy is considered, having the crystallographic axis (a, b, c), then the magnetocrystalline anisotropy depends just on one parameter, θ, the angle between the c-axis and the direction of magnetic moment. The energy is symmetric with respect to the ab plane of the crystal and therefore in the power series just the even power of $sin(\theta)$ are taken into account:

$$\frac{E_{uni}}{V} = K_0 + K_1 \sin^2(\theta) + K_2 \sin^4(\theta) + K_3 \sin^6(\theta) + ... \tag{2.3}$$

Where K_1, K_2, K_3 are second, fourth and sixth order anisotropy constant. In many calculations equation 2.3 is written as a function of $cos(\theta)$:

$$\frac{E_{uni}}{V} = -K_0^{'} - K_1^{'}\cos^2(\theta) - K_2^{'}\cos^4(\theta) + K_3^{'}\cos^6(\theta) + ... \tag{2.4}$$

Using the trigonometric relation $\sin^2(\theta) = 1 - \cos^2(\theta)$ the new coefficient ($K_0^{'}$, $K_1^{'}$, $K_2^{'}$, $K_3^{'}$) can be obtained. Equation 2.4 generates a complicated energy landscape, but in general the numeric values of the anisotropy constant are decreasing with increasing of the order and in many applications just the second order term is considered relevant. The K_0 or $K_0^{'}$ does not have a relevant physical meaning because it simply represents a translation of the reference level.

For cubic anisotropy the expression is more complicated:

$$\frac{E_{cub}}{V} = K_{c0}\left(c_x^2 + c_y^2 + c_z^2\right) + K_{c1}\left(c_x^2 \cdot c_y^2 + c_y^2 \cdot c_z^2 + c_z^2 \cdot c_x^2\right) + K_{c2}\left(c_x^2 \cdot c_y^2 \cdot c_z^2\right) \tag{2.5}$$

Where c_x, c_y, c_z are the direction cosines of the the magnetic moment vector. Depending on the values of K_{c1} and K_{c2} there are different easy axes. In figures 2.5 and 2.4

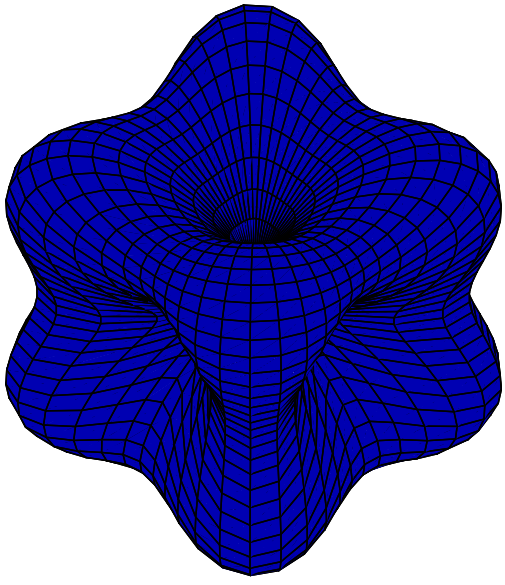

Figure 2.5: Energy distribution for cubic anisotropy: $K_{c1} > 0$ and $K_{c2} = 0$.

the energy density is illustrated for the simplest case of uniaxial and cubic anisotropy.

2.4.2 Shape anisotropy

The orientation of a magnetic moment of a ferromagnetic particle can have preferential orientations due to its shape. Because of the shape, the magnetic moment is under the influence of a field called the demagnetization field. This field generates one or more preferential orientation and can be associated with shape anisotropy. This can simply be explained if we compare the magnetic particle with a magnetic bar. The magnetic bar is symbolically treated like a north and south pole. The magnetic moment is orientated form south pole to the north pole and the magnetic field lines generated by the bar are from the north to south pole. From figure 2.6 it can be seen that inside the bar the magnetic field lines are in opposite direction to the magnetic moment and tries to demagnetize the sample. This field is called demagnetization field and it is present in all the magnetic materials. Using the analogy with the electric polarization, this

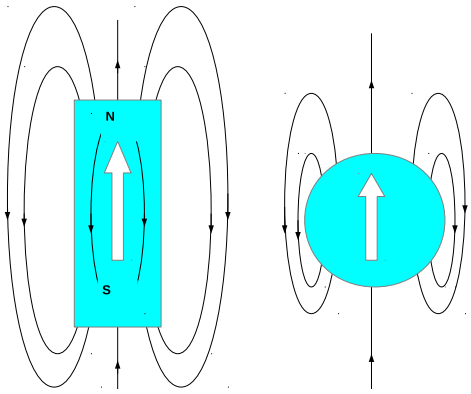

Figure 2.6: Magnetic field line for a magnetic bar and a magnetic particle. The magnetic moment is orientated form south pole to the north pole and the magnetic field lines generated by the bar are from the north to south pole.

field can be interpreted as the field created by the uncompensated “magnetic charges” on the surface. In the direction in which the fictional charges are further away, the demagnetization field is smaller in comparison with the direction in which the charges are closer. As a consequence the sample will magnetize easier on those direction for which the demagnetization field is smaller.

For a general shape the demagnetization field is hard to calculate analytically and it is not constant inside the sample. For an ellipsoid of revolution the demagnetization

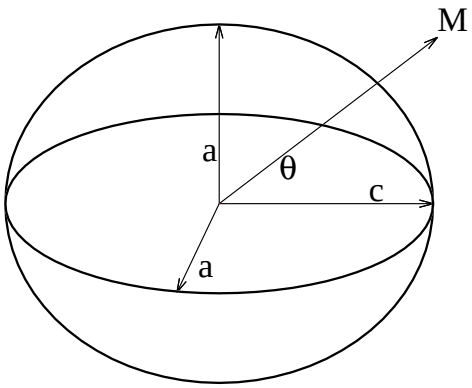

Figure 2.7: A magnetic sample with an ellipsoidal shape, having two semi-axis equal to a and the third semi-axis with c. The demagnetisation field can be calculated for such a sample.

field is uniform inside the sample and Osborn [20] derived the analytical equations. Considering an ellipsoid of revolution with two semi-axis equal to a and the third semi-axis with c (as in figure 2.7), the demagnetization field can be written as:

$$H_d = N_d M_s \tag{2.6}$$

Where N_d is the demagnetization factor for x, y and z direction. N_x and N_y are equal and satisfy (for cgs units) the following equation:

$$N_x + N_y + N_z = 4\pi \tag{2.7}$$

If k_0 is equal to $\frac{c}{a}$ and the Z direction coincide with semi-axis c, then N_z can be calculated from equation 2.8-2.10. The other two demagnetisation factor can be calculated from equation 2.7 using the fact that $N_x = N_y$.

$$N_z = \frac{4\pi}{1-k_0^2}\left[1 - \frac{k_0}{\sqrt{1-k_0^2}} arccos(k_0)\right] \qquad \text{for } k_0 < 1 \qquad (2.8)$$

$$N_z = \frac{4\pi}{3} = N_x = N_y \qquad \text{for } k_0 = 1 \qquad (2.9)$$

$$N_z = \frac{4\pi}{k_0^2-1}\left[\frac{k_0}{\sqrt{k_0^2-1}} arcosh(k_0) - 1\right] \qquad \text{for } k_0 > 1 \qquad (2.10)$$

Base on all the elements presented in this chapter, the energy of a ferromagnetic system can be evaluated. Then the magnetic behavior of the system can be study. In the next chapter, theoretical models for investigating magnetic behaviour are presented.

3

Theoretical Models

3.1 Stoner-Wohlfarth model

The Stoner-Wohlfarth (SW) model describes the magnetisation process of a macroscopic ferromagnetic particle at 0K assuming that all the magnetic moments inside the particle are rotating coherently. This means that all the atomic moment within the particle are parallel with each-other at all time. Therefore the model can be used for mono-domain particles; the change in magnetisation is done by simultaneous rotation of all moments inside the particle. In the study done by Stoner and Wohlfarth [21], they investigate an isotropic ellipsoidal particle, which has a preferred direction due to its shape (shape anisotropy). This is mathematically equivalent to study spherical particles with uniaxial anisotropy as used in this thesis. The equilibrium state is defined by an energy minimum. The SW theory consist in investigating the energy landscape and in determining the energy minima. Considering a spherical particle in an external field, H_{ap}, we can write the energy as sum of magneto-crystalline energy (E_K) and the Zeeman energy (E_H):

$$E_{tot} = E_K + E_H \tag{3.1}$$

$$E_K = -K_1' V \cos^2(\theta) \tag{3.2}$$

$$E_H = -M_s V \vec{e_M} \cdot \vec{H_{ap}} \tag{3.3}$$

Where $\vec{e_M}$ is the versor of the magnetisation vector.

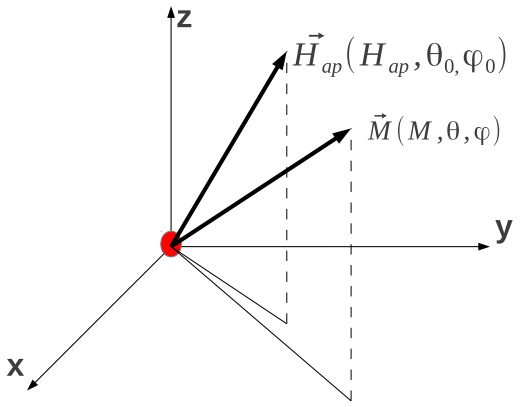

Figure 3.1: 3D representation of the applied field, magnetization vector and easy axis direction. The particle is in the center of the coordinate system and easy axis is on Z direction.

For clarity and simplification of the calculations, it can be demonstrated that this 3D problem can be reduced to 2D without loosing any information, by showing that the easy axis, magnetization vector and applied field direction are in the same plane [22]. For the analytical calculation we will use Cartesian and spherical coordinate systems, considering the easy axis on the OZ direction with the particle in the centre of the coordinate system (as in figure 3.1). The applied field (H_{ap}) and the magnetization vector have the spherical coordinates (H_{ap}, θ_0, φ_0) and (M_s, θ, φ). For the magneto-crystalline energy we will use just the first term in cos from equation 2.4 and we will replace the notation of $K_1^{'}$ with K. Taking into account that the particle size does not change, instead of energy we can use the energy density ($W = \frac{E}{V}$). Under this consideration the previous equations becomes:

$$W_K = -K\cos^2\theta \tag{3.4}$$

$$W_H = -M_s\vec{e_M}\cdot\vec{H_{ap}} \tag{3.5}$$

$$W = W_K + W_H = -K\cos^2\theta - M_s\vec{e_M}\cdot\vec{H_{ap}} \tag{3.6}$$

For a given applied field with fixed direction, the energy density depends on magnetic moment orientation with respect to applied field and to the easy axis. For the equilibrium state, the energy must have a minimum value. Mathematically a necessary

condition for a function to be minimal for a certain point is that the first order derivative with respect to each variable is zero for that point. To prove that the 3 vectors (easy axis, magnetization vector and applied field) are in the same plane, the mentioned condition for variable φ is used. For this we need to rewrite the equation 4.1 as function of angles θ and φ, afterwards forming the derivative with respect to φ.

$$W = -K\cos^2\theta \tag{3.7}$$

$$-M_sH_{ap}\left[\sin\theta_0\sin\theta\cos\varphi_0\cos\varphi+\sin\theta_0 sin\theta\sin\varphi_0\sin\varphi+\cos\theta_0\cos\theta\right] \tag{3.8}$$

$$\begin{aligned}\frac{\partial W}{\partial\varphi} &= -M_sH_{ap}\left[\sin\theta_0\sin\theta\cos\varphi_0(-\sin\varphi)+\sin\theta_0 sin\theta\sin\varphi_0\cos\varphi\right]\\ &= -M_sH_{ap}\sin\theta_0\sin\theta\left[\sin\varphi_0\cos\varphi-\cos\varphi_0\sin\varphi\right]\\ &= -M_sH_{ap}\sin\theta_0\sin\theta\sin(\varphi_0-\varphi)\end{aligned} \tag{3.9}$$

The condition $\frac{\partial W}{\partial\varphi}=0$ and the above relation impose that $\sin(\varphi_0-\varphi)=0$, therefore at energy minimum the easy axis, magnetization vector and applied field must be in the same plane. Taking into account this result, we can consider $\varphi_0=\varphi=0$, reducing

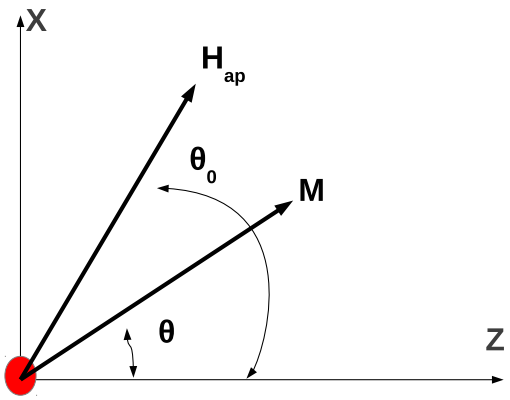

Figure 3.2: 2D representation of the applied field, magnetization vector and easy axis direction. The particle is in the center of the coordinate system and easy axis is on Z direction.

the problem to XOZ plane (the new geometry is represented in fig.3.2). By keeping φ fixed, for describing the entire plane θ will vary from 0 to 2π. The variation of angle

θ in the range $[\pi, 2\pi]$ corresponds in reality to a variation of angle θ in the range $[0, \pi]$ (as it should be),but for $\varphi = \varphi_0 + \pi$. For this case the equation is reduced to:

$$W = -K\cos^2\theta - M_s H_{ap}\cos(\theta_0 - \theta) \tag{3.10}$$

By rearranging the terms, the equation becomes:

$$W = -\frac{M_s}{2}\left[H_K\cos^2\theta + 2H_{ap}\cos(\theta_0 - \theta)\right] \tag{3.11}$$

where $H_K = \frac{2K}{M_s}$ is the anisotropy field.

From analysing the energy dependence of angle θ for different field, it can be observed that there are one or two equilibrium states. Assuming that at first the particle is in a high external magnetic field ($H >> H_k$), the magnetic moment has just one possible state corresponding to the field direction. Decreasing the field, at a specific value a second equilibrium state appears corresponding to a different energy minimum. The magnetic moment deviates from field direction in correspondence to the change in the location of first energy minima. When the field goes to zero the two minima have the same values and the particle moment is blocked in the first state because of the energy maximum between the two states. The difference between the energy maximum and energy minimum is called energy barrier and it is an important property of magnetic materials. Starting to apply a negative field by changing the direction of the field, the energy barrier for the initial state starts to decrease until it disappears and the particle switch to the second state. This corresponds to a significant change in moment orientation. The field when this happens is called critical field (H_{cr}). From a mathematical point of view the point when the switching happens corresponds to an inflexion point, this means that the first and second derivatives are equal to zero. At this field the magnetisation reverses. Up to this point all magnetisation changes have been reversible, but the switching at $H = H_{\mathrm{cr}}$ is an irreversible change.

To find the energy minima and the critical field we need to calculate the first order derivatives with respect to the angle θ ($\frac{\partial W}{\partial \theta} = 0$) and set to zero. This will give the extreme points of the energy function (minima and maxima). To check if the values for θ corresponds to equilibrium states the second order derivative needs to be compared with zero. If it is bigger than 0, the state is in equilibrium. If it is smaller than zero, the

state corresponds to a maximum and if it is equal to zero, the applied field is equal to critical field.

$$\begin{aligned}\frac{\partial W}{\partial \theta} =& \frac{M_s}{2}\Big[H_K 2\cos\theta\sin\theta - 2H_{ap}\sin(\theta_0-\theta)\Big] \\ =& \frac{M_s}{2}\Big[H_K \sin 2\theta - 2H_{ap}\sin(\theta_0-\theta)\Big]\end{aligned} \tag{3.12}$$

$$\frac{\partial^2 W}{\partial \theta^2} \geq \frac{M_s}{2}\Big[H_K 2\cos 2\theta + 2H_{ap}\cos(\theta_0-\theta)\Big] \tag{3.13}$$

To determine the critical field both derivatives need to be equal to zero. This leads to:

$$H_K \sin 2\theta = 2H_{ap}\sin(\theta_0-\theta) \tag{3.14}$$

$$H_K \cos 2\theta = H_{ap}\cos(\theta_0-\theta) \tag{3.15}$$

By dividing the two equation 3.14 and 3.15, $\tan(2\theta) = 2\tan(\theta_0-\theta)$ is obtained and from this equation the projection of magnetic moment on field direction when the switching happens can be calculated. Using equation 3.14 and 3.15, the critical field has the following expression:

$$H_{cr} = \frac{H_K}{g(\theta_0)} \tag{3.16}$$

$$g(\theta_0) = \Big[\sin^{2/3}(\theta_0) + \cos^{2/3}(\theta_0)\Big]^{3/2} \tag{3.17}$$

There is no analytical equation that describes the projection of magnetization on the field direction, but instead the inverse function has an analytical form. To calculate it the substitution $m = \cos(\theta_0-\theta)$ is used, which is the projection of magnetic moment on the field direction normalised to it maximum value. In equation 3.14 $\sin(2\theta)$ must

be written as a function of m:

$$\begin{aligned}\sin(2\theta) &= \sin[-2(\theta_0-\theta)+2\theta_0] \\ &= \sin(2\theta_0)\cos[2(\theta_0-\theta)] + \cos(2\theta_0)\sin[2(\theta_0-\theta)] \\ &= (2m^2-1)\sin(2\theta_0) - 2m(1-m^2)^{1/2}\cos(2\theta_0) \end{aligned} \tag{3.18}$$

Using the above relation in 3.14 the two branches of hysteresis curve are:

$$H_+ = \Big(-m\cos(2\theta_0) - \frac{2m^2-1}{2\sqrt{1-m^2}}\sin(2\theta_0)\Big)H_K \tag{3.19}$$

$$H_- = \Big(-m\cos(2\theta_0) + \frac{2m^2-1}{2\sqrt{1-m^2}}\sin(2\theta_0)\Big)H_K \tag{3.20}$$

Based on these two equations, coercivity and remanence can be calculated. For values of angle θ smaller than $\frac{\pi}{4}$ the switching occurs before *m* reaches zero. In this case the coercivity field and the critical field coincide. For angles bigger than $\frac{\pi}{4}$, the coercivity is calculated from equation 3.19 or 3.20.

$$H_c(\theta) = \begin{cases} \frac{H_k}{g(\theta)} & \text{if } \theta \in [0, \frac{\pi}{4}] \\ \\ \frac{H_k sin(2\theta)}{2} & \text{if } \theta \in (\frac{\pi}{4}, \frac{\pi}{2}] \end{cases} \tag{3.21}$$

From equation 3.20 taking $H_- = 0$ remanence can be calculated.

$$M_r(\theta) = \begin{cases} \sqrt{\frac{1+\frac{1}{\sqrt{1+tg(2\theta)^2}}}{2}} & \text{if } \theta \in [0, \frac{\pi}{4}] \\ \\ \sqrt{\frac{1-\frac{1}{\sqrt{1+tg(2\theta)^2}}}{2}} & \text{if } \theta \in (\frac{\pi}{4}, \frac{\pi}{2}] \end{cases} \tag{3.22}$$

3.1.1 System of particle with spherical random orientation of easy axis

For a system of identical particles with all the easy axes having the same direction all the above calculations from SW model applies, but in a real system, particles have a size distribution, the easy axes are not aligned and also there is a anisotropy constant distribution. At very low temperature (0K as in SW model), distributions of size and anisotropy are not very important. The magnetic properties depend on the mean values. Instead the orientation of easy axis is important. The magnetic behaviour is strongly dependent on the angle of the applied field with respect to easy axis.

In the case of a spherical random orientation of easy axes some properties such as coercivity and remanence can be analytically calculated. For this let us consider a system of identical mono-domain particles with a spherical distribution of easy axes. The probability of having a particle with easy axes in the range $[(\theta,\varphi),(\theta+d\theta,\varphi+d\varphi)]$ is given by:

$$P = \sin(\theta)d\theta d\varphi \quad \text{for} \quad \theta \in [0,\pi] \text{ and } \varphi \in [0,2\pi] \tag{3.23}$$

Where θ is the angle between the easy axis and the applied field. In this case the remanence of the whole system ($\bar{M_r}$) is the mean value:

$$\bar{M_r} = \frac{\int_0^{\pi}\int_0^{2\pi} M_r \sin(\theta)d\theta d\varphi}{\int_0^{\pi}\int_0^{2\pi} \sin(\theta)d\theta d\varphi} \tag{3.24}$$

From the SW model the remanence for one particle is given in equation 3.22. M_r is not dependent on angle φ, therefore $\bar{M_r}$ can be written as:

$$\bar{M_r} = \frac{\int_0^{\pi} M_r \sin(\theta)d\theta \int_0^{2\pi} d\varphi}{\int_0^{\pi} \sin(\theta)d\theta \int_0^{2\pi} d\varphi} \tag{3.25}$$

$$\tag{3.26}$$

Doing the simplification and using the fact that M_r and $\sin(\theta)$ have the same behaviour

in the interval [0, $\pi/2$] and [$\pi/2$, π] The integral becomes:

$$\bar{M_r} = \int_0^{\frac{\pi}{2}} M_r \sin(\theta) d\theta \tag{3.27}$$

Replacing M_r from equation 3.22 we obtain:

$$\bar{M_r} = \int_0^{\frac{\pi}{4}} \sqrt{\frac{1+\frac{1}{\sqrt{1+tg(2\theta)^2}}}{2}} \sin(\theta) d\theta \; + \tag{3.28}$$

$$= \int_{\frac{\pi}{4}}^{\frac{\pi}{2}} \sqrt{\frac{1-\frac{1}{\sqrt{1+tg(2\theta)^2}}}{2}} \sin(\theta) d\theta \tag{3.29}$$

$$\bar{M_r} = 0.5 \tag{3.30}$$

The coercivity is calculated in the same way resulting in: $\bar{H_c} = 0.479 H_k$. All these results from Stoner-Wohlfarth model are used as tests for algorithms developed in this thesis.

3.1.2 Energy barrier

A very important factor in the model is the fact that there are 2 stable states separated by an energy barrier. This aspect leads to more complicated models which have a more realistic description of a real system (as for example including the effect of temperature). A general analytical expression of the energy barrier does not exist, and one needs either to determine it numerically or to use approximations [23]:

$$\Delta E_1(H, \theta_0) = KV \left[1 - \frac{H_{ap}}{H_{cr}(\theta_0)}\right]^{0.86+1.14g(\theta_0)} \tag{3.31}$$

$$\Delta E_2(H, \theta_0) = KV \left[1 + \frac{H_{ap}}{H_{cr}(\theta_0)}\right]^{0.86+1.14g(\theta_0)} \tag{3.32}$$

Where H_{cr} and $g(\theta_0)$ are given in equations 3.16 and 3.17. Numerical implementations used in this thesis are based on the Stoner-Wohlfarth theory and on the above

mentioned equations for energy barriers.

3.2 Temperature effect

Magnetic properties of materials are influenced by temperature. Besides the temperature dependence of some intrinsic parameters like saturation magnetization or anisotropy constant, there are important differences between SW model and experimental measurements. As an example, for a SW particle with anisotropy $K = 5 \cdot 10^5 \text{erg/cm}^3$ and a saturation magnetization of 450 emu/cm^3 (typical values for magnetite) the coercivity field is approximately 1100 Oe, where as in experiments coercivity is temperature and field sweep rate dependent. If the same experiment is repeated at the same temperature but for different field variation rates the hysteresis curves are different. This difference can be explained by the fact that the SW model does not contain temperature effects. In the SW model the magnetic state is well defined by energy minima and the magnetic moment cannot switch to the second minimum until the field is equal to the critical field, however in a real system a particle can receive from the thermal bath enough extra energy to overcome the barrier and switch at a lower field. If the field variation is very slow, then the experimental time is very large and the probability of a particle receiving the extra energy to switch increases and this leads to a decrease of magnetization with time. The dependence of magnetic behaviour with respect to time scale has a large interest in the recording media industry where the time range is very large: from 10^{-12} s, 10^{-8} s (the characteristic time scale for writing on an hard drive) to years (the time scale for storage the written information). For hard disks the time in which the information is stored without being damaged is 10 years [24] [25]. The experimental limitation to time range of seconds or hundreds of seconds, leads to a theoretical and computation investigation. The most used approximation for relaxation time is given by an Arhenius type law:

$$\tau = \tau_0 e^{\frac{\Delta E}{k_B T}} \tag{3.33}$$

where ΔE is the energy barrier between the two possible states, k_B is the Boltzmann constant, $f_0 = \frac{1}{\tau_0}$ is the attempt frequency, having values between $10^{-9} Hz$ and $10^{-12} Hz$. The equation was developed by Arhenius for chemical reactions. Neel [26]and Brown

[27] have developed similar theory for explaining the thermal relaxation or thermal activation. Based on equation 3.33, energy barrier can be evaluated so that at a certain temperature and for a certain time the particle will remain blocked in the initial state. For a particle to remain blocked tens of years it is necessary that $\frac{\Delta E}{K_B T} \gg ln(\frac{t_m}{\tau_0})$. This corresponds to energy barriers 40 times larger than the thermal energy. For hundreds of seconds the energy barrier needs to be at least 20 times bigger than the thermal energy. In general, it can be stated that if the measurement time (t_m) is smaller than the relaxation time, the particle remains blocked and the magnetization curve has a hysteresis type behaviour, but if the measurement time is larger than the relaxation time, the barrier in not sufficient to keep the particle blocked and the particle has a paramagnetic behaviour. In the first case the particle is called ferromagnetic and in the second case is called superparamagnetic. At the limit when ($t_m = \tau_0$) for a given time and volume the blocking temperature can be calculated. Blocking temperature is the temperature at which the transition between ferromagnetic and superparamagnetic behaviour happens.

$$t_m = \tau_0 e^{\frac{\Delta E}{K_B T}} \tag{3.34}$$

Taking logarithms of both sides and rearranging the terms, the blocking temperature becomes:

$$T_B = ln\left(\frac{\tau_0}{t_m}\right)\frac{\Delta E}{K_B} \tag{3.35}$$

Thermal effects introduce random fluctuation and to extract information we need to do averaging over a sample containing a large enough number of particles to have a good statistical results. In a real sample the particles are not identical, each particle having different sizes. If the size distribution is known, then the fraction of superparamagnetic and ferromagnetic particles can be calculated. For zero external magnetic field the energy barrier has the value KV and the critical volume which separated the two types of behaviour is:

$$V_{cr} = ln\left(\frac{t_m}{\tau_0}\right)\frac{K_B T}{K} \tag{3.36}$$

Thermal effects complicates the study of magnetic behaviour and probabilistic approaches such as Monte-Carlo method need to be used. This methods are described in the next section.

3.3 Monte-Carlo methods

There are many methods that use probabilistic means to find exact, non-probabilistic results. In statistics the most used methods are Monte-Carlo (MC) type. The methods are based on generating N random numbers. The function of interest is evaluated for this N points and then the statistic properties of the function are calculated. The accuracy of the method depends on the number of points (N). There are functions which have significant values in a small interval and insignificant values in the rest of parameter space. For example a particle, with the energy landscape illustrated in figure 3.3, will have a higher probability to be in a state near the minima. In the standard Monte-Carlo algorithms the N sample points are selected with the same probability in all the parameter regions. This leads to long time calculations which requires large amount of resources. To improve the algorithm, techniques were developed based on importance sampling, meaning that the sampling of points is not done with uniform probability but according to weighting of the states determined by the probability function. In this case, for the above example there will be more points sampling around the two minima, therefore the numerical calculation will converge faster. Metropolis [28] developed this type of algorithm based on Markov chain. A Markov chain is a transition process between a finite number of possible states. The next state depends just on the current state and not on the previous ones. In this type of process any final state can be achieved from any initial state without having cyclical states. For each scientific field there are a multitude of Monte-Carlo algorithms. In magnetism the most common methods are Metropolis Monte-Carlo and Kinetic Monte-Carlo [29][30][31].

3.3.1 Metropolis approach

If a Stoner-Wohlfarth particle is considered, for a given magnetic field, because of the thermal agitation, the magnetic moment can have any value with a Boltzmann

probability:

$$P(E_{tot}) = \frac{e^{-E_{tot}/k_B T}}{Z} \tag{3.37}$$

where E_{tot} is the total energy of the particle and Z is the partition function and it is calculated from equation 3.38:

$$Z = \int e^{-E_{tot}/k_B T} dE \tag{3.38}$$

The integral is calculated on the whole range of energy values. For a physical system containing a large number of particles, the average value of a macroscopic parameter M (let M be the projection of the magnetisation vector on the field direction) is given by statistical physics as:

$$\langle M(E_{tot}) \rangle = \int M \frac{e^{-E_{tot}/k_B T}}{Z} dE \tag{3.39}$$

This can be calculated if Z is known, but Z is not always known. The algorithm de-

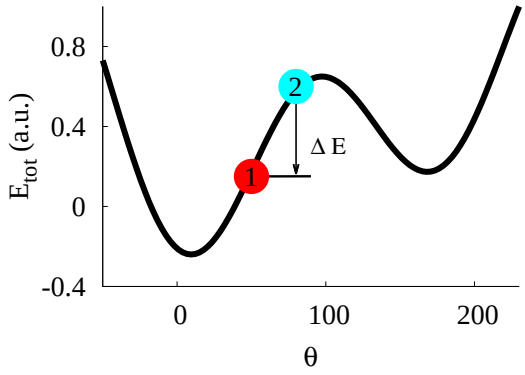

Figure 3.3: Energy as function of θ. The particle magnetic moment can change orientation from state 1 to state 2 with a probability depending on the energy difference of the two states (ΔE).

veloped by Metropolis [28] has the advantage that it gives the average values using a function proportional to the probability, therefore the value of Z is not important. Another advantage is the importance sampling, described in the Metropolis article [28] as

follows: instead of sampling with uniform probability and then weighting the samples with the Boltzmann factor, the sampling can be done with Boltzmann probability and then weighted evenly.

Analysing figure 3.3, representing the energy of a particle for different angles between magnetic moment and the easy axis direction calculated from SW model, the Metropolis algorithm will sample the energy landscape by going from one state to another with a Boltzmann probability characteristic for the energy difference of the two states. If the new state has lower energy than the current one, then the transition always happens. One iteration of the method is summarised as:

1. A particle is selected
2. A new state is generated
3. The difference in energy between the new and current state is calculated
4. The transition probability is calculated based on the equation:

$$P = min\left(1, e^{-\Delta E/k_B T}\right) \quad \text{Where} \quad \Delta E = E_{new} - E_{current} \tag{3.40}$$

5. A random number generated between 0 and 1 is compared with the probability P
6. If P is larger, then the particle goes into the new state else the current state is maintained
7. Steps 2-6 are repeated several times for statistic convergence
8. Going back to step 1 until all the particles are evaluated
9. System average magnetization is equal to the arithmetic average over all the particles

3.3.2 Kinetic Monte-Carlo

The Metropolis MC is used to study equilibrium magnetic properties of a system in contact with a thermal bath. The method does not describe the dynamics of magnetic moment. It assumes that in a long time scale the moment converges towards the equilibrium state. This represents a limitation of the algorithm to the time intervals where dynamics of magnetic moment are not important. Another limitation consists in the fact that there are no real time steps. In this method, time is measured in MC steps (a MC step is described in previous paragraph). Nowak has proposed an updated algorithm called Time Quantificatied Metropolis Monte-Carlo (TQMC) [32] [33] [34], which deals with associating the MC step with a real time. The main equation of the model is:

$$\Delta t_{MC} = \frac{(1+\alpha^2)M_s V}{20 k_B T \alpha \gamma} R^2 \tag{3.41}$$

Where Δt_{MC} represents the time equivalent with a Monte-Carlo step and R is the radius of a cone around the magnetic moment. The new orientation is selected inside this cone and because of this a real time step can be derived. The method was validated by other groups [35]. The cone radius is constrained in between 0 and 1, this leads to the long time scale limit of the model (around milliseconds). The short time domain is limited by the importance of dynamic (around $10^{-8} - 10^{-9}$ s).

For a larger time scale, a different MC method can be used. This algorithm is called Kinetic Monte-Carlo (KMC) and can be applied up to years. In comparison with Metropolis MC, KMC method has real time steps, but can be applied just in cases where the energy barrier is much larger than the thermal energy. The algorithm is based on the assumption that magnetic moment can be just in the states corresponding to minimal energy. If the energy barrier is much larger than the thermal energy, then the particle under the effect of thermal agitation will remain confined in to one of the energy minimum, but if the two energies are close, particle can be with reasonable probability in any state. In the latter case the 2-state approximation is no longer justified and conventional MC must be applied. From a computational point of view this method is more complex because it needs to find the magnetisation states corresponding to the energy minimum and also to calculate the energy barrier that separates these

states.

The basic steps of the algorithm for a given field are:

1. A time step is selected
2. A particle is selected
3. The orientations of magnetic moment corresponding to energy minima is calculated
4. The energy barrier for each state is calculated
5. The transition probability is calculated based on equation[1]:

$$P_2 = (1 - e^{-\frac{t}{\tau}})(1 + e^{-\frac{\Delta E}{k_B T}})^{-1} \tag{3.42}$$

6. A random number generated between 0 and 1 is compared with probability P_2; if the number is smaller than P_2, the new magnetic moment orientation corresponds to minimum 2, else it corresponds to minimum 1.
7. Steps 2-5 are repeated until all particle are evaluated
8. System average magnetization is equal to the arithmetic average over all the particles

The transition probability between the states is given by a set of equation called Master equation. Next, a basic description of Master equations is presented and the probability for a 2 state system is calculated. Master equations are a set of differentiation equations, in which the variation rate of number of particles (or probability) per unit of time from one state to another is equal to the difference between the number of particles arriving in that state and the ones leaving that state. The general Master equations for n possible states have the following form:

$$\frac{dP_i}{dt} = \sum_i [-W_{ik}P_i + W_{ki}P_k] \tag{3.43}$$

[1]the equation and the meaning of each parameter are detailed in the next paragraph

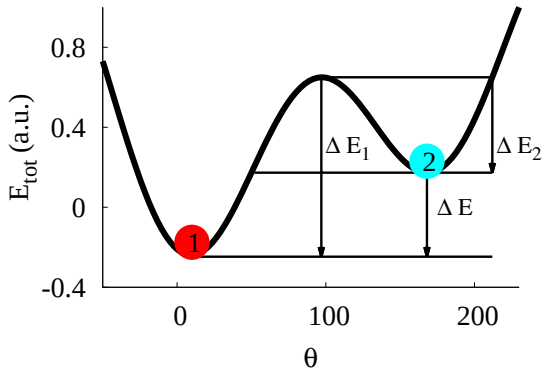

Figure 3.4: Energy as function of angle θ. The particle magnetic moment can have a orientation corresponding just to the two states 1 and 2. ΔE is the energy difference between the states. ΔE_1 and ΔE_2 are the energy barriers corresponding to state 1 and 2.

Where P_i is the probability that the particle is in state 'i' and W_{ik} is the transition rate from state 'i' to state 'k'. One of the conditions that the system must satisfy is that in the long time limit the equilibrium state must be obtained (equation 3.44).

$$\frac{W_{ki}(t \to \infty)}{W_{ik}(t \to \infty)} = \frac{P_{0i}}{P_{0k}} = e^{\frac{E_k - E_i}{k_B T}} \tag{3.44}$$

The system of equations 3.43 is hard to resolve for a general case (n possible states). KMC is using the simplest possible case when $n = 2$. For the following calculations (based on reference [36]) a mono-domain Stoner-Wohlfarth particle with uni-axial anisotropy will be considered. For this simple case the Master equations are:

$$\frac{dP_1}{dt} = -W_{12}P_1 + W_{21}P_2 \tag{3.45}$$

$$\frac{dP_2}{dt} = -W_{21}P_2 + W_{12}P_1 \tag{3.46}$$

Where W_{12} and W_{21} are described by the Arhenius Law.:

$$W_{12} = f_0 e^{\frac{-\Delta E_1}{k_B T}} \tag{3.47}$$

$$W_{21} = f_0 e^{\frac{-\Delta E_2}{k_B T}} \tag{3.48}$$

ΔE_1 is the energy barrier between states 1 and 2. Taking into account that P_1 and P_2 are probabilities and $P_1 + P_2 = 1$, it is sufficient to solve the equation for one probably (P_1) and the second one will be $P_2 = 1 - P_1$. Equation 3.45 can be rewritten to contain just P_1 by replacing P_2 with $1 - P_1$.

$$\frac{dP_1}{dt} = -\frac{P_1}{\tau} + W_{21} \qquad \text{where} \qquad \tau = \frac{1}{W_{12} + W_{21}} \tag{3.49}$$

For a constant external field, W_{21} and τ are also constant. In this case equation 3.49 is a simple ordinary differential equation with the solution:

$$P_1 = W_{21}\tau \left(1 - e^{-\frac{t}{\tau}}\right) + P_1(t=0)e^{-\frac{t}{\tau}} \tag{3.50}$$

Assuming that initially $P_1(t=0)$ is 1, we can write for P_2:

$$P_2 = 1 - P_1 = (1 - W_{21}\tau)\left(1 - e^{-\frac{t}{\tau}}\right) \tag{3.51}$$

Rearranging the terms, the solution can be written as following:

$$P_2 = \left(1 - e^{-\frac{t}{\tau}}\right)\left(1 + e^{-\frac{\Delta E}{k_B T}}\right)^{-1} \tag{3.52}$$

where

$$\Delta E = \Delta E_1 - \Delta E_2 = E_2 - E_1 \tag{3.53}$$

$$\begin{aligned}\tau &= \frac{1}{f_0\left(e^{\frac{-\Delta E_1}{k_B T}} + e^{-\frac{\Delta E_2}{k_B T}}\right)} \\ &= {f_0}^{-1} e^{\frac{\Delta E_2}{k_B T}} \left(\frac{1}{1+e^{-\frac{\Delta E}{k_B T}}}\right)\end{aligned} \tag{3.54}$$

and

$$\begin{aligned}1 - W_{21}\tau &= 1 - \frac{e^{-\frac{\Delta E_2}{k_B T}}}{e^{-\frac{\Delta E_1}{k_B T}} + e^{-\frac{\Delta E_2}{k_B T}}} \\ &= \left(1+e^{-\frac{\Delta E}{k_B T}}\right)^{-1}\end{aligned} \tag{3.55}$$

We can observe that for the long time limit, the solution corresponds to a Boltzmann solution for 2 possible states:

$$P_2 = \frac{e^{-\frac{E_2}{k_B T}}}{e^{-\frac{E_2}{k_B T}} + e^{-\frac{E_1}{k_B T}}} = \left(1+e^{-\frac{\Delta E}{k_B T}}\right)^{-1} \tag{3.56}$$

In this chapter we presented the theory of magnetic behaviour. We started with a 0K model, the Stoner-Wohlfarth theory for a mono-domain particle. Then we discussed the role of the anisotropy vectors distribution, thermal effects and the role of size distribution. At the end of the chapter, Monte-Carlo techniques are introduced. In the following chapter we will use all this information to construct a numerical model that can realistic describe a sample of interacting nanoparticles.

4

Numerical implementation

In this chapter we describe the numerical implementation of our Monte-Carlo model and the algorithms used to solve the inverse problem. The latter one is described in the second part of the chapter. The first part of this chapter describes the model used for simulating magnetic behaviour of interacting magnetic mono-domain particles with uniaxial anisotropy.

4.1 Magnetic simulation

A 3D system with periodic boundary condition containing N particles is considered. The particle positions are randomly generated for different packing fraction. To mimic a real system log-normal distribution of size and anisotropy values are considered and also the easy-axes are random oriented. The algorithm based on Stoner-Wohlfarth (SW) model, consists of using the Metropolis and Kinetic Monte-Carlo methods. The energy of one particle, *i*, from the system has a SW like expression (equation 3.1):

$$E_{i,tot} = -K_i V_i \cos^2 \theta_i - M_s V_i \vec{e_M} \cdot \vec{H_{i,eff}} \tag{4.1}$$

Where the $H_{i,eff}$ is the effective field acting on particle i. The effective field consists of the external field and the magnetostatic interaction field.

4.1.1 Particle position generation

To obtain a system of random particles position having a certain packing fraction we start with a perfect simple cubic lattice with a large lattice spacing so that there no overlapping. Then the particles are randomly moved inside a sphere of radius D_{max} with a Monte-Carlo approach. This is done calculating for each particle E_{old} and E_{new} based on equation:

$$E_{new,old} = \sum_j 1000 \cdot (\frac{d}{r_{new,old}})^4 \tag{4.2}$$

Where the sum is done over all the neighbour particles. d is the particle diameter and r_{new} and r_{old} are the interparticle distances after and before the random move. The terms in the sum are dimensionless energies of a repulsive potential. This repulsive potential forces the particles to move apart. Normal Monte-Carlo approach is used: if the new energy is small than the old one, then the move is accepted, else the move is accepted with a probability $P = e^{(-\Delta E)}$. This step is repeated 50 times and then the system size and the particle distance are reduced with an amount so that there are no touching particles. The procedure is repeated until the desired packing fraction is obtained. Afterwards 500 more random moves are done for each particle.

4.1.2 Interaction field

To include magnetostatic interaction, the shape of the sample, packing density and particle arrangement inside the sample must be taken into account [31][37][38]. The interactions are included through the effective field which contains the dipole field generated by all the particles:

$$\vec{H_i} = \sum_{\substack{j \\ j \neq i}} \frac{M_s V}{4\pi\mu_0 r_{ij}^3} \left[\frac{3}{r_{ij}^2} (\vec{e_{Mj}} \cdot \vec{r_{ij}}) \vec{r_{ij}} - \vec{e_{Mj}} \right] \tag{4.3}$$

Direct summation approach is impracticable because of the time resources needed to compute the interaction for all the particles in real system. The method scales with N^2. A general used approach consists of calculating the dipole field in a small region

around the particle and replacing the rest of the field with a mean field equivalent to the demagnetization field described in section 2.4.2 [39]. For this, around a particle a sphere of radius R_c is considered. The sphere must be much smaller than the sample size and larger than the average interparticle spacing. The interaction field can be expressed as the sum of the dipole interaction field of all the particles inside the sphere, the demagnetisation field and the Lorentz cavity field (as illustrated in figure 4.1). The latter one handles the double counting of interaction inside the sphere. The effective

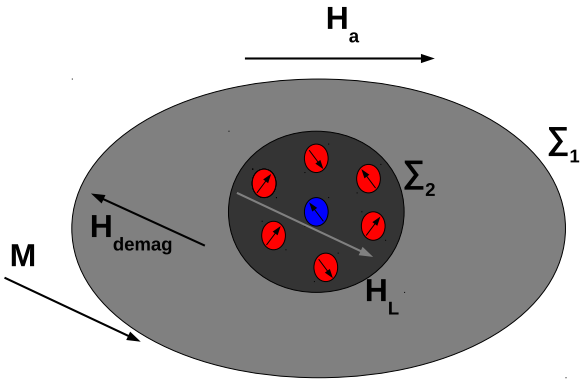

Figure 4.1: The effective field acting on the blue particle. Σ_1 is the surface for which the demagnetization field (H_{demag}) is calculated, Σ_2 is the Lorentz cavity surface for evaluating the Lorentz field (H_L) and with red are represented the particle inside the cavity that determine the dipole field acting on the blue particle. M is the average magnetic orientation of the entire sample and H_{ap} is the applied field.

field can be written as:

$$\vec{H_{i,eff}} = \vec{H_{ap}} + \vec{H_{dem}} + \vec{H_L} + \vec{H_{dip}} \tag{4.4}$$

where:

$H_{i,eff}$ is the total field acting on particle i

H_{ap} is the external field

H_{dem} is the demagnetization field

H_L and the Lorentz field

H_{dip} is the dipole field generated by the particles inside the cavity and it can be calculated using equation 4.3

For the simulations presented in this thesis R_c is chosen to be sufficiently large, so that it does not affect the results. Magnetization curves are generated for different values of R_c, then R_c is chosen to be the smallest value for which there is no significant change in the results.

4.1.3 Periodic boundary condition

To simulate real samples the system is considered at the centre of the sample and periodic boundary conditions (PBC) must taken into account to exclude the small size edge effect. With PBC we create a extended system by translating replicas of the computational cell in 3D. For 3D system this consist of 26 copies. In figure 4.2 the idea is represented for simplicity in a 2D system but the consideration are the same as in 3D. The initial system is placed in the middle and the rest of them, labelled from 1

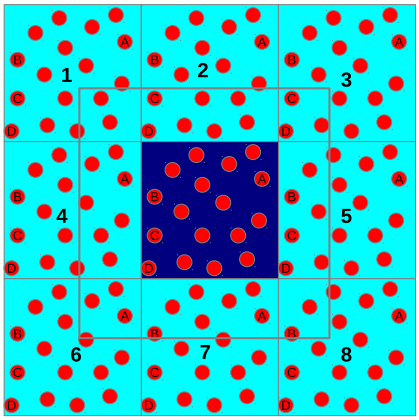

Figure 4.2: Periodic boundary condition for a 2D system. All the calculation are done just for the central system; the replicas, labeled from 1 to 8, are used just for calculating the dipole field to exclude the edge effects.

to 8, are copies of the initial systems and translated in all directions. All the calculation are done just for the central system; the replicas are used just for calculating the dipole field. R_c must be smaller than half of the system so that no particle should be taken into account twice.

4.1.4 Numeric implementation of the model

The aim of this thesis is to investigate the influence of dipole interaction on the magnetic behaviour of nanoparticle systems and also to directly link the simulation with experimental results allowing extra information about the system to be obtained. The time interval that corresponds to the general used experimental devices (such as VSM-Vibrating Sample Magnetometer and SQUID-Superconducting QUantum Interface Device) implies that KMC method should be used. This method has a good description of real behaviour if the energy barrier is much larger than the thermal energy, so that the states corresponding to energy minima are taken into account. In a real system particle sizes are not uniform, they follow a distribution like log-normal distribution. If a system containing spherical particles with mean diameter (dm) of 6.6 nm and anisotropy constant equal to $5 \cdot 10^5 \text{erg/cm}^3$, then for a measurement done at 20K with measurement time of 1 minute the critical volume (as described in section 3.2 by equation 3.36) is $1.37 \cdot 10^{-19} cm^3$. This corresponds to a particle diameter of 6.4 nm. All the particles with diameter smaller than $6.4nm$ will have superparamagnetic behaviour. While $\frac{KV}{k_b T}$ is relatively large the KMC approach is necessary, since the use of the normal Metropolis MC fails to achieve quasi equilibrium in a reasonable CPU time. However, as $\frac{KV}{k_b T}$ decreases the 2-state approximation inherent in the KMC method breaks down and the standard MC method becomes necessary. We take a cut-off value of $\frac{KV}{k_b T} = 3$ to define the boundary between the use of the MC and KMC methods. In the model implemented by me both type of behaviour, ferromagnetism and superparamagnetism are included by using KMC and MC methods as implemented by Chantrell in 2000 [9]. If the energy barrier of a particle in zero field, KV, is larger than 3 time the thermal energy, $k_B T$, then the KMC is used, else the Metropolis MC is used. When KMC is used, a few Metropolis MC step are also considered. This is done to have a better thermal equilibration inside the minima. Even if the energy barrier is large in comparison with the thermal energy, states very close to the minima are possible with a reasonable probability. Metropolis MC steps will include this aspect into the simulation.

To generate the magnetization curves a linear time dependence of external magnetic field is considered. The sweeping rate of the field will be:

$$R = \frac{\Delta H}{\Delta t} \tag{4.5}$$

A continuous time variation of field increases the difficulty of solving the Master equations. The magnetic behaviour in a field variation can be describe by solving the Master equations iteratively. For small time intervals (Δt), the field can be approximated to a constant value and the solution from Master equations presented in chapter 3 can be used. At the next time step the field is updated to the new value and Master equations are used again. In chapter 3 the two algorithms are defined formally. Next the main steps of the practical implementation are presented.

1. All the parameters values are initialised
2. Particle position is generated
3. The time step is selected and the corresponding applied field is considered
4. A particle is selected and the effective field acting on that particle is calculated using equation 4.4
5. The ratio $\frac{KV}{k_BT}$ is calculated
6. If $\frac{KV}{k_BT}$ bigger than 3, The Kinetic MC is used:
   (a) The magnetic moment orientation corresponding to the two minima is calculated
   (b) The energy barrier is calculated using Pfeiffer approximation [1]
   (c) The probability is calculated based on following relation [2]:

$$P_2 = (1 - e^{-\frac{t}{\tau}})(1 + e^{-\frac{\Delta E}{k_BT}})^{-1} \tag{4.6}$$

   (d) A random number generated between 0 and 1 is compared with probability P_2; if the number is smaller than P_2, the new magnetic moment orientation corresponds to minimum 2, else it corresponds to minimum 1.
7. If $\frac{KV}{k_BT}$ is less than 3, the Metropolis MC is used:

[1] The equation is presented in chapter 3
[2] All the parameters from this equation are define in chapter 3

(a) A new state is randomly generated

(b) The difference in energy between the new and current state is calculated

(c) The transition probability is calculated based on the equation:

$$P = min\left(1, e^{-\Delta E/k_B T}\right) \quad \text{Where} \quad \Delta E = E_{new} – E_{current} \tag{4.7}$$

(d) A random number generated between 0 and 1 is compared with the probability P

(e) If P is larger, then particle goes into the new state else the current state is maintained

8. If KMC was used, a few Metropolis MC steps are also used

9. The steps 4-8 are repeated until all the particles are considered

10. The average magnetization is calculated

11. The steps 3-10 are repeated until all the field values are considered

We can use the Monte-Carlo model to observe the system behaviour for different parameters; this is called forward problem and is generally applied in the magnetism community. In this thesis we are focusing on the inverse problem which consist of obtaining the system's parameters from the known results.

4.2 Inverse problem

In this section we present a methodology by which the microscopic parameters describing magnetic nano-particle system can be accurately determined by solving the inverse problem for experimental data using simulated magnetization curves. Simulated curves are obtained using the approach presented in previous section.

The inverse problem is solved by using 2 different methods. Both methods can be used to obtain information about the magnetic properties of a system from experimental magnetisation loops. The methods have the same general mathematical background

and this is curve fitting. The idea of curve fitting is to have a specific fitting function or a mathematical model and to find the specific coefficients (parameters) which make that function match data as closely as possible. First method called Grid Search Method (GSM) involves setting up a grid in fitting parameters space and evaluating the ”goodness of the fit” at each grid point. This method scales with the numbers of grid points and number of fitting parameters and also makes the general interpretation, beside finding the best fit, less accessible for a parameter space greater than 2. Second method involves an adapted Levenberg–Marquardt algorithm (LM) used by most of the fitting software [40]. For using this method we need a function that describe how close are the data we simulate with the data we are investigating. This function is the sum of squared errors (χ^2). A short description of fitting is presented in appendix A on page 84. All the fitting algorithms are not trivial for non-linear models and the Monte-Carlo model we used for simulating the magnetic behaviour is clearly non-linear. The problem that arises in this situation is the interpretation of the results:

1. Is the solution unique?

2. How accurate is the solution?

3. What are the errors of the solution?

The first problem involves the way of finding the best fit. The function that describes the goodness of the fit is χ^2 and depends on the parameters we are interested in finding; the method consists in finding the minimum of this function. For our model as in the non-linear models there may be the possibility of χ^2 having more than one minimum. The solution may be describing, instead of a global minimum, a local minimum and then the results are not the desired ones. The second problem refers to a qualitative way of evaluating the goodness of a fit. Because the date are subjective to errors, there is a chance that a good fit may result because of the errors and not of actual agreement between the model and the data. The third problem consists in the fact that errors will depend on the χ^2 landscape near the global minimum. If there is a large almost flat region around the minimum, then the errors are too large for the results to be meaningful. Also in our case the situation is even more complicated. Besides the errors from experimental data, our Monte-Carlo method also contains statistical errors because of the thermal effects included.

The first issue will be our subject of investigation in the next chapters, whereas for the other two we can use mathematical conditions for χ^2. Because of the thermal fluctuation there is a probability Q that the data may fit the model due to chance. For a given confidence level $(1-Q)$ there is a upper limit value for χ^2 (χ^2_{lim}) for which the agreement between the data and the model are acceptable with $1-Q$ confidence. A confidence level of 1.0 corresponds to perfect agreement between the data and the model, and a value of 0.0 corresponds to a complete disagreement between those two. In general values about 0.5 are considered relevant. For determining the errors there are similar considerations. The errors are related to the variation of χ^2 around the best fit value, therefore $\Delta\chi^2$, the difference between χ^2 for a given set of parameters and the χ^2 of the best fit, is used. Both χ^2 and $\Delta\chi^2$ depends on the degrees of freedom, which for χ^2 is equal to the difference between the number of data points and the number of fit parameters and for $\Delta\chi^2$ is equal to the number of fit parameters. All of the above are discussed in more details in the appendix A on page 84.

The results will be presented for simplicity with χ^2 and $\Delta\chi^2$ normalised to the limit value, χ^2_{lim} and $\Delta\chi^2_{lim}$ respectively. For the normalised χ^2_{norm} ($\chi^2_{norm} = \frac{\chi^2_{norm}}{\chi^2_{lim}}$) the condition will be $\chi^2_{norm} < 1$. In the next chapters we will refer to χ^2_{norm} and $\Delta\chi^2_{norm}$ without using the subscript "norm". In tables 4.1 and 4.2 are given some values for the two function for different degrees of freedom and for different confidence level. The results will be presented with 50% confidence level for χ^2 and 99% confidence level for $\Delta\chi^2$. Next the two methods used in this thesis are presented.

confidence level	degrees of freedom			
	1	2	3	4
50%	0.45	1.39	2.37	3.36
90%	2.71	4.61	6.25	7.78
95%	3.84	5.99	7.81	9.49
99%	6.63	9.21	11.34	13.28

Table 4.1: The value for $\Delta\chi^2_{lim}$ for different confidence level and degrees of freedom.

confidence level	degrees of freedom			
	79	99	159	199
50%	78.33	98.33	158.33	198.33
90%	95.48	117.41	182.24	224.96
95%	100.76	123.22	189.42	232.91
99%	111.14	134.64	234.01	281.87

Table 4.2: The value for χ^2_{lim} for different confidence level and degrees of freedom. The value degrees of freedom corresponds to 2 fit parameters and some typical number of data points we used.

4.2.1 Levenberg–Marquardt method

The first method uses the least square fitting approach to find the optimal parameters, **p**, from a set of data. Levenberg-Marquardt (LM) is a standard way to handle nonlinear least square fitting (e.g. used by Origin, Matlab). The process of finding the best possible values of parameters that describe a set of data is iterative. This is done by finding the minimum of χ^2 with a combination of two methods: Gradient descent method and Gauss-Newton method. Gradient descent works very well if the χ^2 is far from minimum and uses the gradient to find the direction in which χ^2 has the largest decrease. The second method is for the case when the parameters **p** are very close to the minimum and assumes a quadratic form of χ^2 as function of the fitting parameters. Both methods require the derivative of the model output with respect to the fitting parameters. λ controls the iteration process. If λ is small LM is more similar with grid search method and the new value for **p** is a large step in the direction of the steepest decrease χ^2. If λ is large, then Gauss-Newton method dominates and the new value of **p** correspond to the minimum of the quadratic approximation of χ^2.

For the description of the LM algorithm, f(x) is used to mathematically describe the model. We can write χ^2 as:

$$\chi^2 = \sum_{i=1}^{N} \left[\frac{m_i(H^i_{ap}) - f(H^i_{ap}, \mathbf{p})}{\sigma_i} \right]^2 \tag{4.8}$$

Where **p** represents the fitting parameters, $m_i(H^i_{ap})$ is the value of the normalized magnetisation ($m_i = M_i/M_s$) to be fitted at H^i_{ap} and $f(H^i_{ap}, \mathbf{p})$ is the value of function at

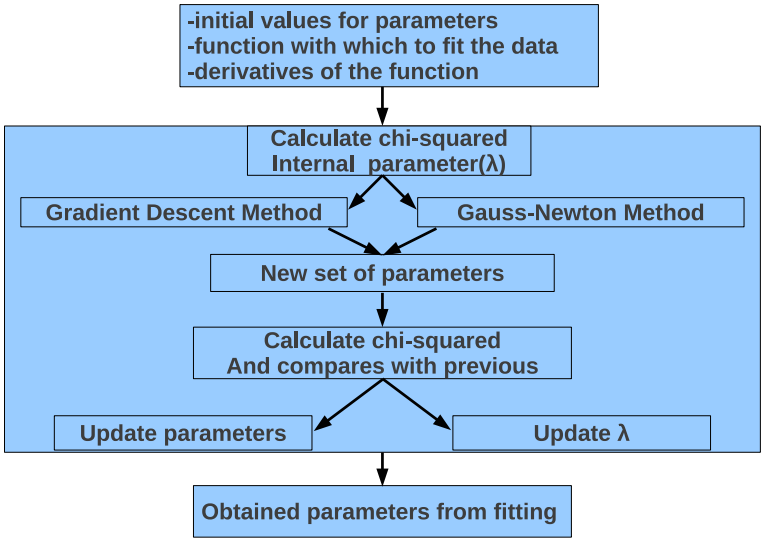

Figure 4.3: Schematic representation of the LM fitting algorithm.

H^i_{ap} for a given value of parameters. σ_i is the standard deviation of errors for m_i. The result of fitting are the values of fitting parameters (**p**) that describe the data best. The basic idea about how this method works can be observed from figure (4.3). At the beginning you need to specify the initial value of fitting parameters, the fitting function and its derivative with respect to the fitting parameters. Then the χ^2 is calculated and based on the internal parameter, λ, a combination of two methods for finding a better estimation of parameters is used. A new set of fitting parameters are generated and the χ^2 is calculated again; if the new value of χ^2 is smaller than the old one, λ decreases, else λ increases. To achieve the best fit is necessary an iteration of this steps, with the mention that when λ decreases the new values of parameters replace the previous one.

To illustrate how the entire methodology (LM + Monte-Carlo simulation) works, we will present next a practical example. For this example and for the test and validation of the methodology, instead of experimental data, reference data from simulation are used. In this way all the parameters are well controlled and we know what results the method should output. We consider a system of log-normal distributed spherical particles with a mean diameter (dm) of 6.7 nm and a standard deviation of 15%. The easy axes are spherically random orientated with anisotropy value of $3 \cdot 10^5$ erg/cm^3 and standard deviation of 10%. The saturation magnetization is 400 emu/cm^3. The ex-

ternal field is applied up to 5000 Oe with a field sweep rate of 1.0 Oe/s and a field step of 100 Oe. For this example the hysteresis loop was simulated for a non-interacting system at 10K. The reference loop was obtain from averaging over 100 independent simulations and the loops used in the LM fit are averaged over 5 simulations.

To calculate the standard deviation of errors, σ_i, needed for χ^2 we used the following relation:

$$\sigma_i = \sqrt{\frac{1}{N-1}\sum_{j=1}^{N}(\overline{m}_j^i - m_j^i)^2} \tag{4.9}$$

Index i corresponds to the points on the loop for each field and index j corresponds to each loop from the N (N=100) loops generated. The reference loop is the average over the 100 loops and it corresponds to $\overline{m}_j^i$ ($\overline{m}_j^i = \overline{M}_j^i/M_s$). For this example we consider that σ_i has a constant value of 0.01. Latter we will show what are the effects of this simplification on the results and on the interpretation of the fit. We will consider that anisotropy and saturation magnetization are the unknown magnetic parameters and the described LM algorithm is used to obtain these values ($\mathbf{p} = (K, M_s)$). In figure 4.4 is presented the magnetization curves for the initial values of parameters used in the fitting, for the real parameters and the magnetisation curves for the best fit parameters.

First we need to give some starting values for K ($1 \cdot 10^5$ erg/cm^3) and M_s (100 emu/cm^3) as input to the LM algorithm. With this values a hysteresis loop is generated and the a initial value of χ^2 is computed. The magnetization loop for this parameters is represented in figure 4.4 with blue points. For calculating the new estimated values for the fit parameters, the derivatives of the magnetisation curves as a function of these parameters are needed. In contrast to fitting to an analytical function where the value of the function and its derivative have well defined values, our numerical model is susceptible to errors. The derivatives need to be calculated numerically and they will also be subject to errors. These errors will contribute to the errors of the fit. For calculating the derivatives we used the three point method (equation 4.10). In the next chapter we will investigate if using a more refined method for calculating the derivative

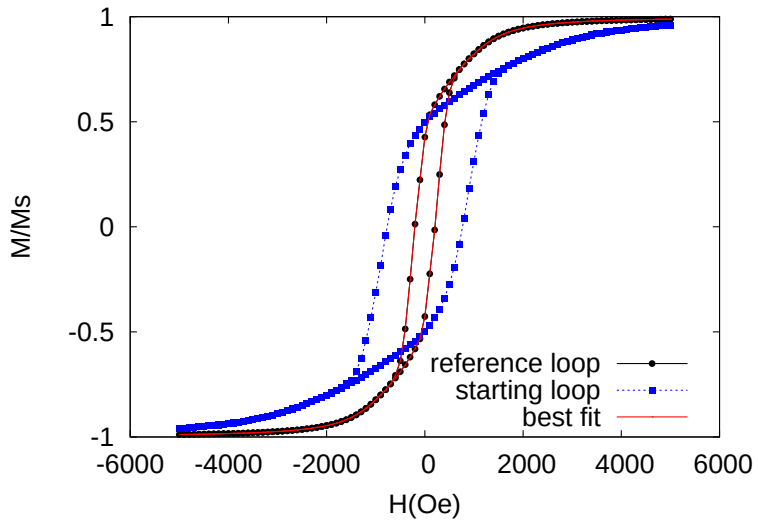

Figure 4.4: Hysteresis curves for the reference loop, the starting loop and the best fit loop. All the loop are for non interactive system with dm=6.7nm, $\sigma_{dm} = 15\%$, $\sigma_K = 10\%$ at 10K. The reference loop has K= $3 \cdot 10^5$erg/cm^3 and $M_s = 400$emu/cm^3, the starting loop has K= $5 \cdot 10^5$erg/cm^3 and $M_s = 300$emu/cm^3 and the fit loop has K= $3 \cdot 10^5$erg/cm^3 and $M_s = 400$emu/cm^3.

is more appropriate.

$$\frac{df(H^i_{ap}, p_j)}{dp_j} = \frac{f(H^i_{ap}, p_j + \Delta p_j) - f(H^i_{ap}, p_j - \Delta p_j)}{2\Delta p_j} + Err(H^i_{ap}, \Delta p_j) \qquad (4.10)$$

Where p_j is the parameter for which the derivative is calculated and Δp_j is the step chosen for calculating the derivative. For this, magnetization curves are simulated with values of K and M_s around the current estimation values and equation 4.10 is used. Δp_j is chosen to be 10% of the current values of each of the fit parameters. After this is computed, new values for K and M_s is obtained. Then a new value for χ^2 is calculated and compared with the previous one. If the χ^2 is lower, meaning that the loop are more similar, the two parameters are updated to the new values and λ is decreased. Else the old values are maintained but λ is increased. Derivatives give the direction for the largest decrease in χ^2 and λ controls the step in that direction. A small λ correspond to a large difference between the old and the new estimation of the parameters and favours the gradient descent method. On the other hand a large λ favours the second

method. The entire algorithm is repeated until a small enough χ^2 is obtained or the change in parameters produces an insignificantly different value for χ^2. In table 4.3 the iterative values for K and M_s are given as well as χ^2 corresponding to that value and if the movement is accepted or not. The final results consists in the values for the

number of iteration	**K** $(\mathbf{10^5 \cdot erg/cm^3})$	$\mathbf{M_s}$ $(\mathbf{emu/cm^3})$	χ^2	$\chi^2_{\mathbf{norm}}$	λ	**accepted rejected**
1	5.000	400.0	121795.52	614.10	10.0	-
2	4.826	313.3	97118.55	489.68	1.0	accepted
3	4.131	363.3	30516.83	153.86	0.01	accepted
4	3.200	388.6	1129.22	5.69	0.001	accepted
5	2.999	397.8	3.56	0.018	0.0001	accepted
6	3.012	402.4	1.69	0.008	0.00001	accepted
7	3.016	399.2	2.74	0.014	0.0001	rejected
15	2.997	399.7	0.87	0.004	0.1	accepted

Table 4.3: The iteration process of fitting the reference loop with LM. The normalisation factor corresponds to 50% confidence level for 201 points on the magnetisation curve and 2 fitting parameters.

best fit parameters and also the errors for determine them. For this examples K is 2.997 $\cdot 10^5$ $\frac{erg}{cm^3}$ with an error of 0.061 $\cdot 10^5 \frac{erg}{cm^3}$ and M_s is 399.7$\frac{emu}{cm^3}$ with an error of 13.4 $\frac{emu}{cm^3}$. K and M_s are obtain with a confidence level of 50% and the error are calculated for 99% confidence level. The only element that remains to be determined is the uniqueness of the solution. If there is more than one minimum value for χ^2 the uniqueness is not satisfy and LM algorithm is strongly dependent of the initial parameters. To investigate this last issue we use Grid search method, which will be presented next.

4.2.2 Grid Search method

For the Grid Search approach we use the MC model of the nanoparticle arrays to generate a large set of hysteresis loops for different K and M_s values (not restricted to these however, the method can be used for other quantities) in a broad interval around the expected values. Then the experimental hysteresis curve is compared with every such hysteresis loop available in the look-up table and the sum of squares of errors χ^2(K, M_s) is calculated in every case. Thus, the result is a table of χ^2(K, M_s)

values. The minimum $\chi^2_m = min(\chi^2(K, M_s))$ from all K and M_s is the best-agreement computational loop, which corresponds to the values of K and M_s from the look-up table describing the data best. We also calculate error-bars for the best K and M_s based on the 99% confidence interval statistics, i.e. by selecting all (K, M_s) pairs for which the value of $0 < \Delta\chi^2_{norm} < 1.0$. For 2 parameters a 2D map can be generated for a graphic visualisation of the solution. This method cannot be applied for the entire parameter space. A interval of interest needs to be considered and the calculations are done for a finite discretization in that interval. The optimal values and the error are determined with a certain precision depending on the level of discretization. This method is equivalent to the LM+MC method from the previous section for sufficiently refined divisions of values of K and M_s used for generating the look-up table. Its advantage is that it provides more insight into the physics as it allows to visualise the uniqueness of the solution and the K-M_s parameter correlation. A quantitative investigation of parameter correlation is not presented in this thesis as it is not the subject of our investigation, but a qualitative description of the correlation is offered by the Grid search method. If similar variation of the parameters is observed in the $\Delta\chi^2$ plot, then the two parameters are positively correlated. If opposite variation is observed, then the parameters are negatively correlated and if one parameter does not effect the other, then there are no correlations.

Next we will present a practical example for the grid search method. The same system and the same reference loop is used as in the LM example from previous section. K and M_s will be also in this case the parameters we want to obtain. To apply this second method a large set of hysteresis loops for different K and M_s values in broad intervals around the expected value needs to be generated. The interval for K and M_s is given by physical properties of the system investigated. In this case we are interested in magnetite nanoparticles. The interval of interest for K is between 0.2 and $5 \cdot 10^5$erg/cm^3 and for M_s is between 80 emu/cm^3 and 560 emu/cm^3. The grid is generated with a step in K of $2 \cdot 10^4$erg/cm^3 and a step in M_s of 20 emu/cm^3. The experimental loop (in this example the reference loop illustrated in figure 4.4) is compared with all the loops generated and χ^2 is calculated for each loop. The results are for constant σ_i equal to 0.01 as in LM example. For the above example a 2D map of $\chi^2(K, M_s)$ and $\Delta\chi^2(K, M_s)$ is illustrated in figure 4.5. In figure 4.5a the map for the normalised value of $\chi^2(K, M_s)$is represented with respect to the value corresponding to 50% confidence interval. This

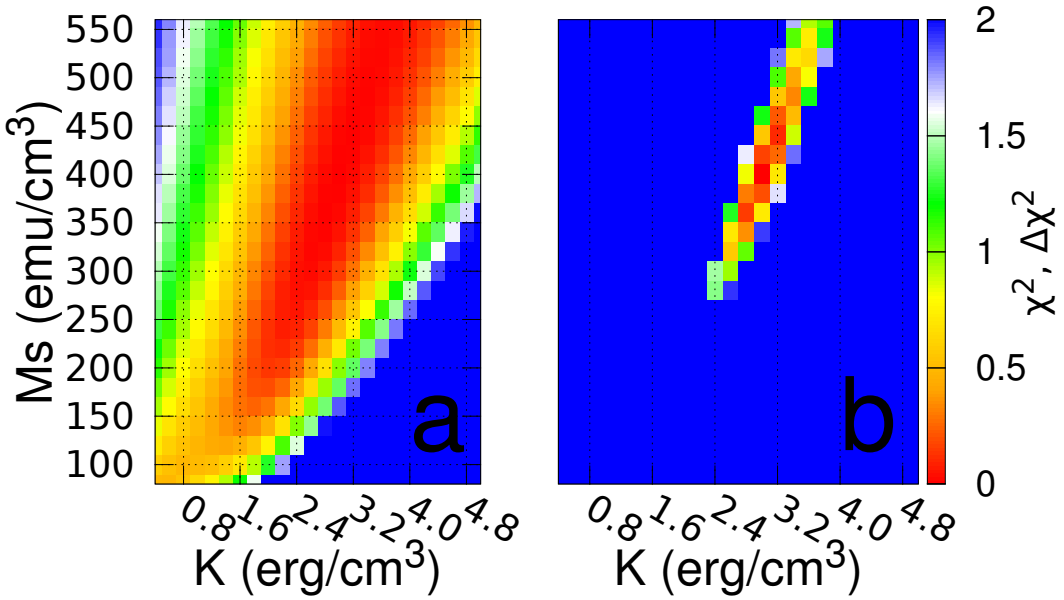

Figure 4.5: χ^2 and $\Delta\chi^2$ grid for finding the reference loop. a) $\chi^2(K, M_s)$ for 50% confidence interval. b)$\Delta\chi^2(K, M_s)$ for 99% confidence interval. The optimum value for K is $5 \cdot 10^5$erg/cm^3 and for M_s is 300 emu/cm^3. K and M_s are positive correlated.

contains information about the uniqueness of the solution and goodness of the fit. The colours red and yellow are for χ^2_{norm} smaller than 1. χ^2_{norm} can vary in a large range as it can be seen in table 4.3. For clarity all the values above 2 are illustrated with blue with the mention that in that region there is no local minimum. From the same figure it can be seen that K and M_s are positively correlated. Figure 4.5b illustrates the map for $\Delta\chi^2$ normalised to the 99% confidence interval value. This contains information about the optimal parameters, the errors of the optimal parameters and about the correlations between parameters. The values of $\Delta\chi^2_{norm}$ smaller than 1 contains the value of the fit parameters for which the model describes the reference loop with 99% confidence. It can be seen from figure 4.5b that the errors for K and M_s are large. K can be between $2.5 \cdot 10^5$erg/cm^3 and $3.7 \cdot 10^5$erg/cm^3. The interval for M_s is between 300emu/cm^3 and 550emu/cm^3. All the results are presented for normalized value of χ^2 and $\Delta\chi^2$ and for simplicity of the notation we will discarded the subscript ”norm”.

In this chapter we presented the numerical algorithm used for generating the magnetisation curves and the two methods used for solving the inverse problem. For the Monte-Carlo algorithm, to simulate an interacting system we need to take into account the sample shape, the geometry of particle arrangement and the particle size and distribution. The grid search method and the Levenberg–Marquardt were presented as used in this thesis. For calculating χ^2 a constant value of σ_i equal to 0.01 is considered and for Levenberg–Marquardt the numerical derivatives are calculated with 3 point method. In the next chapter we will investigate the implication of this two consideration. This is done in the second part of the chapter. The first part consist in testing the Monte-Carlo algorithm.

5

Validation of the algorithms

The implementation of the magnetic behaviour (the Monte-Carlo code) and the inverse problem algorithms (the Levenberg–Marquardt and Grid Search methods) are developed in the Fortran programming language. The calculations were carried out on Wohlfarth, one of the Computational Magnetism Group clusters available at the University of York. The cluster contains 24 Compute Nodes with various CPUs (AMD Phenom II X4 945/925, Intel Core i5, AMD Athlon II X4) with various RAM sizes. We will outline that the programs are not very demanding from the point of view of hardware resources and could be run on a personal computers.

Due to the nature of the Monte-Carlo algorithm, any further improvement to the performance of the Monte-Carlo code (for example using parallel computing or GPUs) was not possible. Therefore, to speed up the calculation of the entire methodology we study the efficiency of the inverse problem algorithms. This is briefly discussed in section 5.2.

5.1 Validation of the Monte-Carlo algorithm

Before using the algorithm to investigate the effect of interactions and to compare the simulations with experiments, a set of tests to validate the numerical methods must be considered. For the Monte-Carlo algorithm simulating the magnetic behaviour, the results from numerical calculation are compared with analytical expressions. Because the effect of interactions are very hard to study analytically, the tests will be done for

a non-interacting system. The interaction fields were calculated for different configurations and compared with other calculations to confirm that interactions are properly determined in the simulations.

5.1.1 Comparing with Stoner-Wohlfarth model

One standard test is to compare the result with the Stoner-Wohlfarth model (SW) in very low temperature limit ($T << 1K$). For this test a non-interacting system of spherical particles with 6.7 *nm* diameter, anisotropy constant of $5 \cdot 10^5$erg/cm^3 and saturation magnetisation $M_s = 456$ emu/cm^3 was used. If we consider identical particles with all the easy axes having the same direction, then for small temperatures, the SW behaviour for one particle with the same parameters values should be obtained. In figure 5.1 is illustrated the simulated hysteresis curves at 0.01K for different values of angle θ, which is the angle between the easy axis and the applied field. The curves reproduce very well the hysteresis loops from SW model.

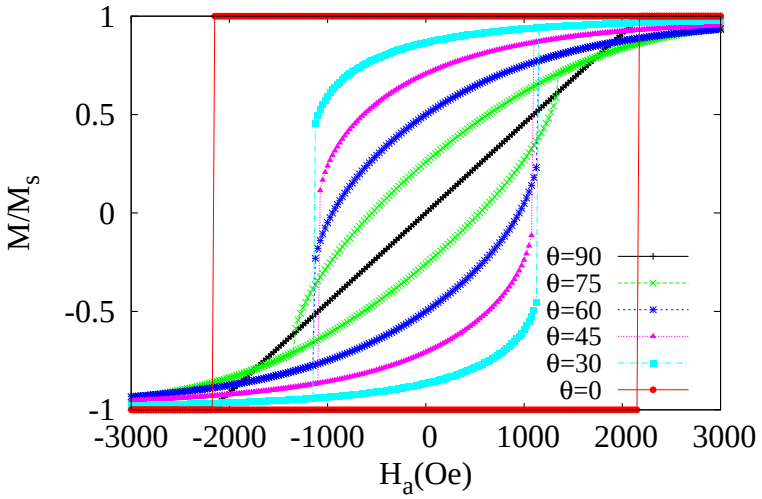

Figure 5.1: Hysteresis curves for identical particles with dm=6.7 nm diameter, K= $5 \cdot 10^5$ erg/cm^3, M_s= 456 emu/cm^3 at 0.01 K for different angles between the easy axis and the applied field. The loops are in agreement with SW theory.

In the SW model the coercivity field and remanence was calculated as function of the angle θ. If we compare the coercivity obtained from simulations with the analytical

expression 3.21, we can see from figure 5.2 that the values are in good agreement. The same comparison can be made for remanence (figure 5.3), for which the angle

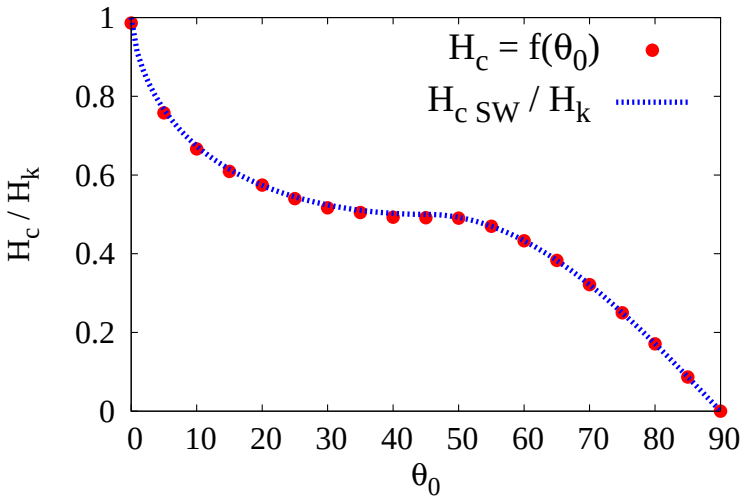

Figure 5.2: Coercivity field as function of angle θ at T = 0.01K. The blue points are the values from simulations and they are in good agreement with the analytical result (dash blue line). Error bars are smaller than the dots and cannot be seen.

dependence is given by equation 3.22.

The last comparison that we can make with the SW model is in case of random orientation of easy axes. In figure 5.4 is illustrated the simulated hysteresis curve for this case using the same values of parameters: K = $5 \cdot 10^5$erg/cm^3, $M_s = 456$ emu/cm^3. The coercivity field is 1068Oe approximately the same value as from the SW model, 1050Oe. Also the remanence magnetisation 0.504M_s is in good agreement with the theoretical model 0.5M_s.

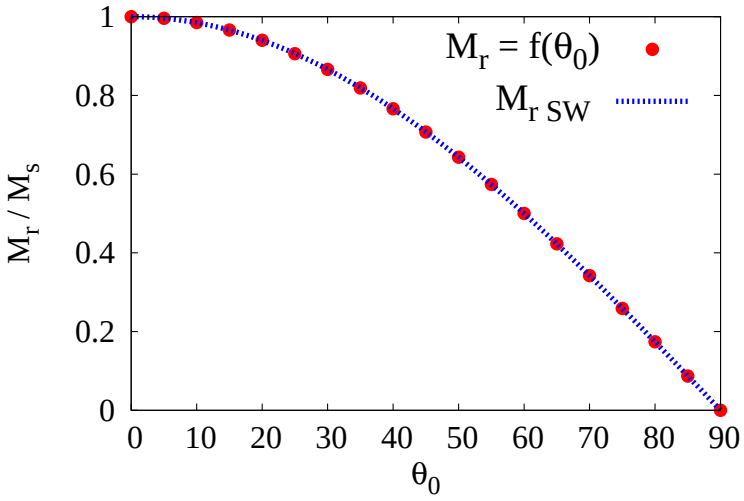

Figure 5.3: The remanence magnetisation as function of angle θ at T = 0.01K. The blue points are the values from simulations and they are in good agreement with the analytical result (dash blue line). Error bars are smaller than the dots and cannot be seen.

5.1.2 Coercivity field as function of sweep rate

To include the thermal effect a different validation needs to be used. One of the tests is comparing the simulation results with an equation that describes the behaviour of the coercivity field as function of the sweep rate of the applied field. This was first found empirically by Sharrock [41] in 1987 and one year latter the equation was derived theoretically by Chantrell [42]. This relation was used for studying magnetic recoding media [43]. The equation has the following form:

$$H_C = H_K(1 - \sqrt{\frac{ln(t\,f_o)}{\beta}}) \tag{5.1}$$

where

$$t = R^{-1}\frac{H_K}{2\beta}(1 - \frac{H_C}{H_K})^{-1} \tag{5.2}$$

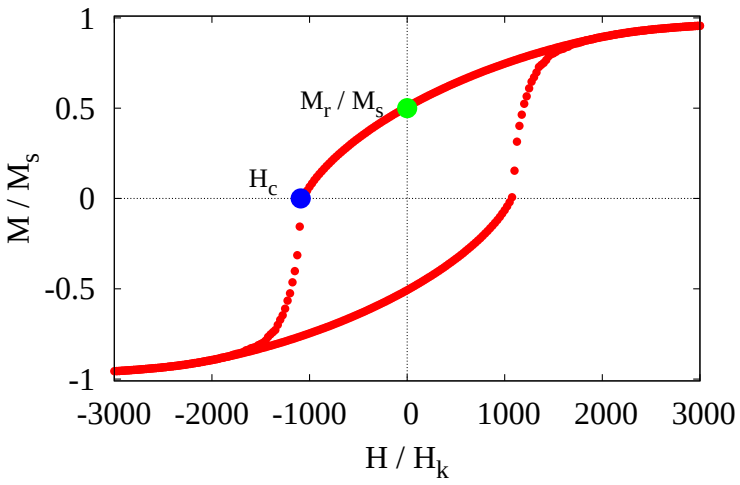

Figure 5.4: Hysteresis curve for a system of identical particles with random orientation of easy axes for K = $5 \cdot 10^5$erg/cm^3, $M_s = 456$ emu/cm^3 and $T = 0.01K$. The coercivity field from simulation (blue dot) is 1068 Oe approximately the same value as from the SW model, 1050 Oe. The remanence magnetisation from simulation (green dot) is $0.504M_s$ and it is in good agreement with the theoretical model $0.5M_s$.

and

$$\beta = \frac{KV}{K_B T}$$

Equation 5.1 is transcendental and it is easier to write the logarithm of sweep rate as function of coercivity.

$$ln(R) = \frac{ln(f_0 H_K)}{2\beta} - ln(1 - \frac{H_C}{H_K}) - \beta(1 - \frac{H_C}{H_K})^2 \tag{5.3}$$

In the theoretical paper [42] a very important assumption was used. The assumption is that the transition from a positive magnetisation to a negative one is very sharp. For this reason the simulations were done for easy axes aligned with the field direction. In figure 5.5 the theoretical curves and the calculations from simulations are illustrated for 1 and 10K. The data from simulations is in good agreement with the analytical result.

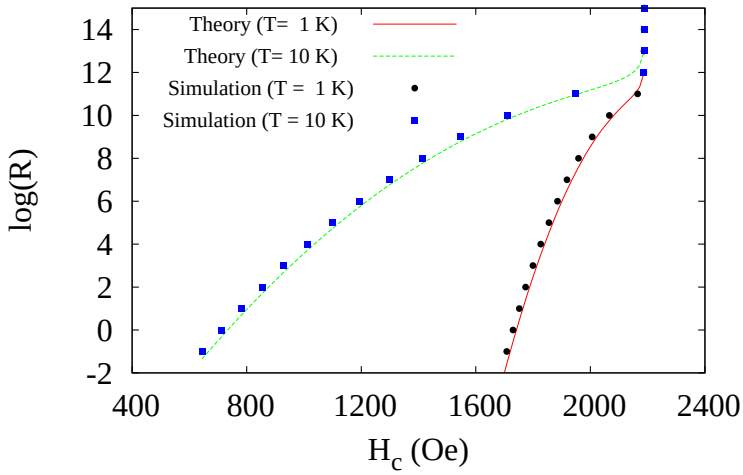

Figure 5.5: $log(R) = f(H_c)$ for a system of identical particles with random orientation of easy axes for K = $5 \cdot 10^5$erg/cm^3, $M_s = 456$ emu/cm^3 and $\theta = 0$. The simulation results (black dots for 10K and blue squares for 1K) are in agreement with analytical calculations (dash green line for 10K and red line for 1K).

5.1.3 Validating the combined KMC and MC method

To test the combined KMC and MC method in the superparamagnetic limit we can compare the simulation with numerical integration of the equilibrium state.

$$\bar{M} = \frac{\int_0^{\pi}\int_0^{2\pi} \cos(\alpha)\sin(\alpha) e^{\frac{-E}{k_b T}} d\alpha d\beta}{\int_0^{\pi}\int_0^{2\pi} \sin(\alpha) e^{\frac{-E}{k_b T}} d\alpha d\beta} \tag{5.4}$$

Where α and β are the spherical coordinate of the moment direction, with the field on the Z direction. E is the energy of the particle and it is given by equation 3.1. To include any type of distribution like size distribution, anisotropy distribution or easy axis distribution will make the integral 5.4 more complicated to solve. For this reason we will test the model for a system of non-interacting identical particles, with dm = 6.7 nm, K = $3 \cdot 10^5$erg/cm^3, M_s = 400 emu/cm^3. The applied field rate is 1 Oe/s with field

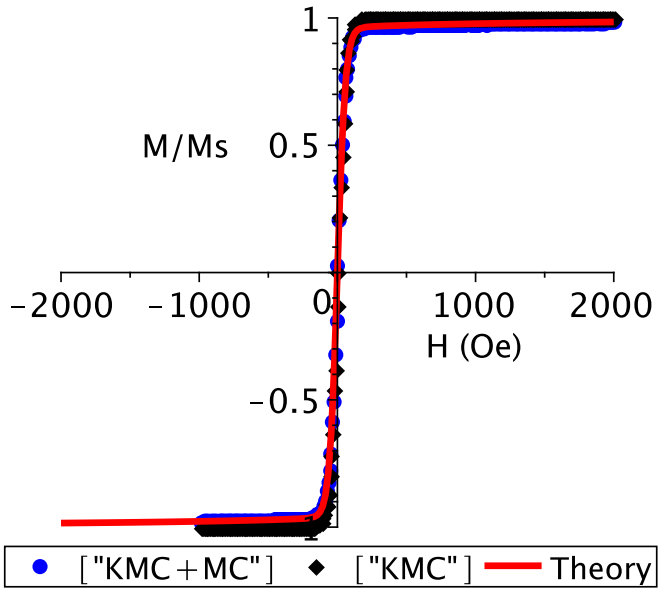

Figure 5.6: Magnetisation curves for identical particles with dm=6.7 nm, K = $3 \cdot 10^5$erg/cm^3, M_s = 400 emu/cm^3, R=1 Oe/s, $\Delta H = 10$ Oe at 25K. The results from the numerical integration of equation 5.4 (red line) are described accurately by the the combine method KMC+MC (blue dots) and also by the KMC method (black diamonds).

step of 10 Oe. We did the calculation for different angles between easy axis and the applied field, varying between 0 and $\pi/2$. We will present just the result for angle equal to zero, but the conclusions are similar for the rest of the angles. We will compare the combined KMC and MC algorithm used in this thesis with the KMC algorithm and the numerical integral of equation 5.4 (referred to as "theory" in the following).

As mention in section 4.1.4 the limit where the algorithm switches from KMC to MC is $\frac{KV}{k_bT} = 3$. For values larger than 3, KMC is applied but a few MC steps are also used for a better equilibration. To validate the method we will chose different temperatures so that the $\frac{KV}{k_bT}$ ratio will vary from a relative large value to values smaller than 3. For this example we vary the temperature from 25K to 125K in steps of 25K. For large ratio of $\frac{KV}{k_bT}$ all three methods are in good agreement as it can be seen for T = 25K, $\frac{KV}{k_bT} = 13.69$, in figure 5.6. But as the ratio decrease the difference are more

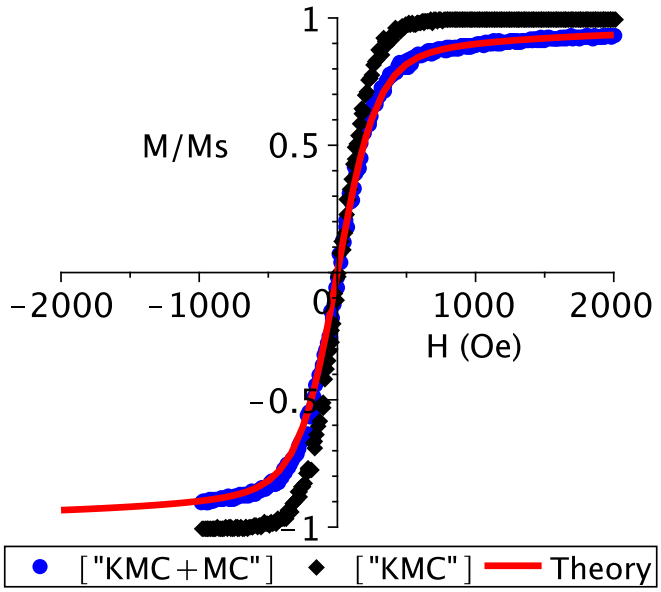

Figure 5.7: Magnetisation curves for identical particles with dm=6.7 nm, K = $3 \cdot 10^5$erg/cm^3, M_s = 400 emu/cm^3, R=1 Oe/s, $\Delta H = 10$ Oe at 100K. The easy axis is parallel with the field direction. The results from the numerical integration of equation 5.4 (red line) are described accurately by the the combine method KMC+MC (blue dots), whereas using just the KMC method the results (black diamonds) diverge.

significant. For 100K and 125K which is just above and under the limit value of 3 ($\frac{KV}{k_bT} = 3.42$ and 2.74) the result are illustrated in figure 5.7 and figure 5.8. Using just the KMC method the results do not describe the real behaviour. To properly describe the superparamagentic limit the combined KMC and MC method need to be used.

In conclusion we tested our model in the low temperature limit by comparing with the Stoner-Wohlfarth theory. Then we tested the KMC method using the Chantrell equation for coercivity as function of field rate. Finally we validated the combined KMC and MC method to have a better description of the superparamagnetic behaviour.

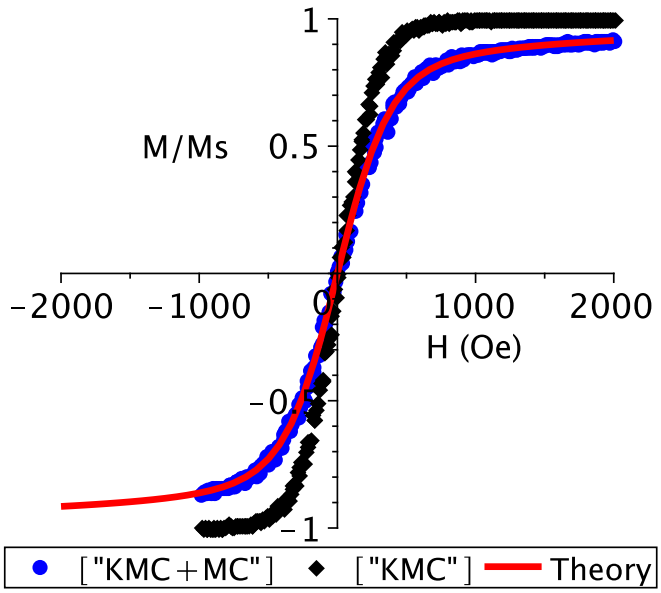

Figure 5.8: Magnetisation curves for identical particles with dm=6.7 nm, K = $3 \cdot 10^5$erg/cm^3, M_s = 400 emu/cm^3, R=1 Oe/s, ΔH = 10 Oe at 125K. The easy axis is parallel with the field direction. The results from the numerical integration of equation 5.4 (red line) are described accurately by the the combine method KMC+MC (blue dots), whereas using just the KMC method the results (black diamonds) diverge.

5.2 Validation of the inverse problem algorithms

In the previous chapter we presented the Grid search method (GSM) and the Levenberg–Marquardt (LM) algorithm using two approximations. First approximation is that we consider a constant value for σ_i when we calculated χ^2 for both methods. For LM we calculated numerically the derivative of the magnetisation curve with respect to the parameters of interest using the three point method. The reason for choosing this approximations is that we wanted to construct the simplest approach that is still very powerful. Before using this approximations we need to test them.

First we will focus on the effect of constant σ_i. If we analyse figure 5.9 where σ_i is calculated for the reference loop using equation 4.9, we can observe that 0.01 is an overestimation. The calculations are redone taking properly into account the

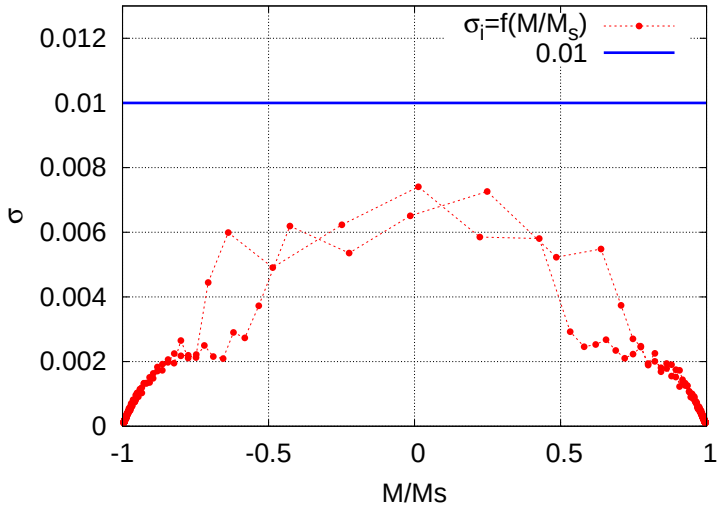

Figure 5.9: σ_i for each point on the loop for the reference loop for K=$3 \cdot 10^5$ erg/cm^3 $M_s = 400$ emu/cm^3. The value 0.01 is a overestimation of the σ_i (red dots).

errors and the result from the grid search method is illustrated in figure 5.10. The optimal values for K and M_s remain the same, but the error of the two parameters are smaller than in the previous case. Now M_s is between 350 and 450 emu/cm^3 and K is between 2.7 and $3.3 \cdot 10^5$erg/cm^3. Also the correlation between parameters remains the same as in the case with constant $\sigma = 0.01$. The reason for this is that in general the

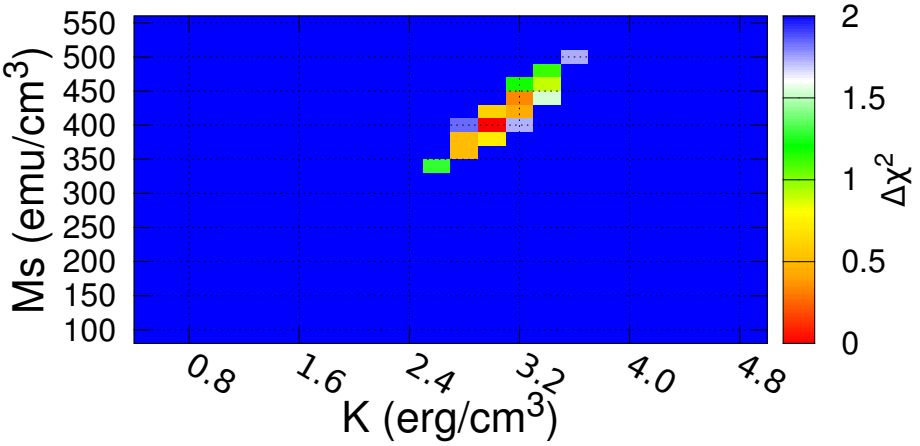

Figure 5.10: $\Delta\chi^2(K, M_s)$ for 99% confidence interval and with σ_i calculated from equation 4.9. The optimum value for K is $5 \cdot 10^5$erg/cm^3 and for M_s is 300 emu/cm^3. The errors are smaller as using a constant value of 0.01 for σ_i.

landscape for χ^2 remains the same and the minimum corresponds to the same value of K and M_s. The only difference consists in the actual value of χ^2 and the exact determination of the goodness of the fit. We did this comparison for different sets of reference loop generated. Calculating σ_i from equation 4.9 and using the constant value of 0.01 provides good results.

After applying the Grid search method and confirming the uniqueness of the solution we can validate the LM and discuss the importance of using a constant value for σ_i and the efficiency of calculating the derivative with the 3 (equation 4.10) or 5 (equation 5.5) point method. For the above reference loop we used the LM method with:

1. constant σ_i and using the 3 point method for computing the derivatives
2. constant σ_i and using the 5 point method for computing the derivatives
3. σ_i calculated for each point on the loop using equation 4.9 and using the 3 point method for computing the derivatives
4. σ_i calculated for each point on the loop using equation 4.9 and using the 5 point

method for computing the derivatives

$$\frac{df(p_i)}{dp_i} = \frac{-f(p_i+2\Delta p_i)+8f(p_i+\Delta p_i)-8f(p_i-\Delta p_i)+f(p_i-2\Delta p_i)}{12\Delta p_i} + Err(\Delta p_i) \tag{5.5}$$

For the initial values of the fit parameters (K and M_s) we used 3 values for K (10^5erg/cm^3, $2.5\cdot10^5$erg/cm^3 and $5\cdot10^5$erg/cm^3) and 3 values for M_s (100 emu/cm^3, 300 emu/cm^3 and 600 emu/cm^3) to cover the parameter space in the region of interest. In total there are 9 different loops as the starting point for the fit and 4 LM approaches. In all the cases the best fit values are within 1% of the actual values. The errors from LM are less than 20 emu/cm^3 for saturation magnetization and less than $1\cdot10^4$erg/cm^3 (for non-interacting system, with interaction the errors are larger), but there is a difference between the errors from using constant σ_i data and including σ_i correctly. If we use equation 4.9 the error of the parameters of interest are smaller than if we use a constant σ_i equal to 0.01. Using $\sigma_i = 0.01$ we overestimated the errors of the reference data as it can be seen in figure 5.9 and therefore a overestimation of the errors in obtaining the two parameters is expected. For this particular reference loop the errors in determining K and M_s are $0.061\cdot10^5$erg/cm^3 and 13.4emu/cm^3 using constant σ_i, where using with the proper value of σ_i at each data point the errors are smaller: $0.026\cdot10^5$erg/cm^3 for K and 3.7emu/cm^3 for M_s. The actual value of σ_i depends on magnetisation (figure 5.9). However, using a constant σ_i that overestimates the actual value gives reasonable results.

For calculating the derivative with respect to the fit parameters the 5 point method is more accurate than the 3 point method, but a higher accuracy does not mean necessarily that the solution converges faster. Both methods output, in the error limit, the same optimal value for the fit parameters. We investigated the number of loops needed to be generated for the result to converge for different reference loops and different starting loops using the two methods for calculating the derivative. In both cases the number of iterations is similar, but the first method needs $4\cdot M_f+1$ loops per iteration and the second one needs $2\cdot M_f+1$ loops per iteration, where M_f is the number of fit parameters. For M_f=2 (as the example above) using the 5 point method, 9 loops must be generated and for the 3 point method just 5 loops. On average using both method of

calculating the derivatives requires 20 iteration, that means using the 3 point method requires 80 fewer loops to be simulated. If M_f is larger, then the difference between the two methods increases. For the LM method the first approach with constant σ_i and using the 3 point method for computing the derivatives is the best option, because it is faster and requires less information about the data.

We did this investigation systematically for different values of K and M_s at different temperature and including also interaction. The results are similar with the above example. In conclusion, using constant σ_i provides good results. For all the results presented in this thesis the minimal value of χ^2 is at least 2 order of magnitude smaller than the limit value for 50% confidence (as it can be seen in table 4.3). For this reason all the result have at least a 50% confidence for the goodness of the fit, although a graphic visualisation or a different method can be used (for example the R^2 test). For all the cases studied, the errors are larger for both K and Ms if a constant value of 0.01 is used for σ_i. For a constant σ_i smaller than 0.01 the previous statement is not true. For this reason we chose to use σ_i equal to 0.01.

6

Results

In this chapter we apply the methods developed so far to study data obtained from experiments, in particular to analyse experimental magnetization curves measured at different temperatures. This is a typical example of the identification problem, where given a particular measurement type we want to go 'backwards' from the measured data and learn about the physical properties of a system, i.e. solve the inverse problem. There are two main questions that need to be addressed when applying similar approaches for the inverse problem. The first question relates to the uniqueness of the inverse problem. In other words, when the model is fitted to the magnetization curve data, are the model parameters uniquely identified from the fitting procedure? In many cases, it turns out that the inverse problems are ill-posed and there exists an wide range of model parameters describing the same experimental data. In this case, the solution set is incomplete and full identification of the parameters cannot be achieved. The second question relates to the applicability of a model in describing experimental samples. If the model is insufficient to describe the measurement data, then the fits are of low quality. That leads to a large value of the sum of squared errors (χ^2). However, it is possible that even if small χ^2 values are found, the identified model parameters may show systematic deviations from the expected values. Such cases are usually hard to deal with, and can only be understood by performing robust statistical analysis of a broader set of experimental data of a different nature. For example, in addition to magnetization curves, the magnetization versus temperature measurements, or magnetization versus time relaxation decay experiments, may also be required.

6.1 Description of experimental data used for identification

We first describe the properties of measurement data sets, which will be quantified below in terms of the developed identification procedure. The samples were prepared and magnetization curves were measured by the group led by Prof. Sara Majetich at the Physics Department, Carnegie Mellon University in Pittsburgh, USA. The sample contains spherical magnetite nanoparticles with a non-magnetic surfactant shell organised in a distorted hexagonal closed packed structure. The transmission electron microscopy (TEM) imaging gave the mean diameter (dm) of the spheres as 6.7 nm with a standard deviation of 15% and a packing fraction of approximately 0.33. We note that the magnetic core may be smaller than the spheres as seen from TEM. The magnetisation versus field curves were measured by the superconducting quantum interference device (SQUID) in the geometry shown in figure 6.1, for a set of 8 different temperatures: 10K, 35K, 60K, 85K, 110K, 135K, 160K and 185K. During the measurement, the external magnetic field was oriented perpendicular to the sample holder shown in figure 6.1. The maximum external field value was 10000 Oe and the field sweep rate was 0.8 Oe/s.

6.2 Basic setup of the Monte-Carlo model for identifying the properties of experimental data

We now use the experimental information given in previous section to reduce the number of fit parameters necessary for the optimisation procedure. The identification of the model parameters will be based on the magnetisation versus field data sets (magnetization curves). In the real sample magnetostatic interactions are present. For the model to be realistic, geometric aspects of the sample needs to be included:

1. The shape of the sample
2. The packing fraction of the system
3. Position of the particles

Figure 6.1: Sample geometry. The sample contains spherical magnetite nanoparticles with mean diameter of 6.7 nm and a a standard deviation of 15%. The packing fraction is 0.33 and the particles are covered in a non-magnetic surfactant shell.

The shape of the sample gives rise to a demagnetising field as described in section 2.4.2, which is an important contribution to the effective field acting on particles in the sample. Similarly, the packing fraction and the particle positions contribute to the local variation of the effective field, thus influencing the magnetic behaviour of a sample. To include the shape of the experimental sample in the model we approximate the overall geometry by an ellipsoid of revolution with principal axes $a = b \neq c$. In this case the demagnetising field is defined simply by a ratio c/a, following chapter 2.4.2, and adds a mean-field contribution to the effective field, which is uniform through out the sample. Due to the simple form of the demagnetising field expression (equation 2.6 and 2.8-2.10 in section 2.4.2), the ratio c/a can be interpreted as a fit parameter, in the sense that its optimal value can be found during the fitting routine. Including the particle sizes and positions into the optimisation routine is far less simple due to the presence of inter-particle interactions. For a non-interacting system the particle position is irrelevant and the particle size can be included into the fitting in a straightforward way. However, if interactions are present, accurate positions of particles need to be included if dipole interactions are to be described realistically. The magnetic behaviour of a particle is sensitive to the local magnetostatic field acting on it. This

field can lead to a ferromagnetic or antiferomagnetic behaviour depending on neighbour particles position [44] [45]. This is nontrivial for randomised samples, such as with disordered positions of particles or clustered samples, where changing the particle size directly affects the local variation of the packing fraction and thus the local variation of the dipole interaction fields contributing to the overall magnetisation behaviour. Generating randomised particle distributions requires dedicated algorithms, such as described in section 4.1.1, which would need to be sequentially executed during the optimisation procedure if the particle size (or position) was included as a fit parameter, thus making the approach computationally very demanding. Due to these complications, the particle size has not been chosen as a direct fit parameter. Instead, for developing our analysis, a preference was given to pre-generating realistic particle size and position distributions. We wanted to encompass the expected values for the experimental samples described above. For this we generated systems for several different packing fractions, such that in all cases the mean particle diameter was 6.7 nm and the standard deviation of the particle size distribution varied from 0 to 25%. Furthermore, the complicated geometry of the sample as shown in figure 6.1 could not be fully specified and for this reason to quantify the demagnetising fields we chose two different approximate limits: the case with c/a = 1 (spherical geometry) and c/a = 0 (thin film geometry), roughly consistent with the experimental data described above.

Another requirement is the need to calibrate the computational model. In experiments, magnetization curves are typically measured in terms of the absolute magnetic moment, whereas our Monte-Carlo code computes magnetization curves in terms of the magnetisation M(H) normalised by the saturation magnetisation M_s, as is standard in computational physics. To calibrate the computational data, we first obtain normalisation factors by fitting to the experimental data the well-known 'approach to saturation law' of the form [46, 47, 48]:

$$m(t) = M(H)V_t = M_s V_t \left[1 - \frac{A}{H} - \frac{B}{H^2} - \frac{C}{H^3}\right] + DH + E\sqrt{H} \tag{6.1}$$

where V_t is the magnetic volume of all the particles in the sample. As the name suggested, 'approach to saturation law' describes the behaviour of magnetic moment in high field regime which corresponds to the approach to saturation value of the magnetic moment. Equation 6.1 and the coefficient A, B, C, D and E result from an under-

lying theory and include the effects of stress, anisotropy, interaction, inhomogeneities and other factors. Not all of these coefficients may be relevant - depending on the type of a sample under study. In the present case of the experimental data introduced in section 6.1 the above equation reduces to a simpler form:

$$m(H) = M_s V_t \left[1 - \frac{F}{H^G}\right] \tag{6.2}$$

which then allows the value of $M_s V_t$ to be extracted for the calibration between the experimental and computed data. In figure 6.2 the normalise experimental magnetization

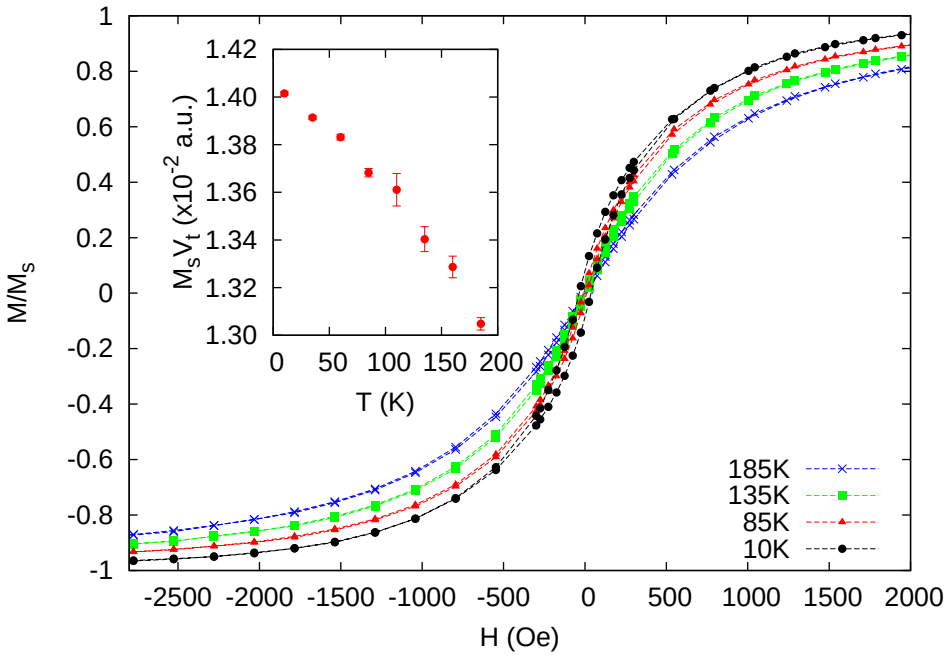

Figure 6.2: Normalised experimental magnetization curves for sample A at 4 temperatures (10K, 85K, 135K, 185K). The points represent the normalize experimental data and the lines are for guidance. The normalisation factor $M_s V_t$ for each temperature is shown in the inset.

curves as function of field for the sample are illustrated for 4 different temperatures: 10K, 85K, 135K and 185K.

6.3 Identification problem: An example of the study of uniqueness properties of a model

In the previous section we set up the Monte-Carlo model aided by available information about the experimental samples. The physical variables which were not measured directly were the mean anisotropy constant and the saturation magnetisation, which will be used as fitting parameters. While experimental techniques to measure K and M_s are available, it is generally desirable to be able to identify K and M_s directly from measured magnetization curves. The standard deviation of anisotropy constant, σ_K, is also an unknown variable. We consider a log-normal distribution of anisotropy. This is the standard technique in describing a system of nanoparticles. We tested different values of σ_K in the interval $[0, 30\%]$ and these values do not change the result for these experimental data. A value of 10% is chosen for σ_K.

We want to find K and M_s for the experimental samples from the measurement data described in section 6.1. The Monte-Carlo model presented in section 4.1.4 is used as the reference model. But first we will consider the question of uniqueness. This question relates to studying the inverse solutions of the model, i.e. whether every computed magnetization curve corresponds to a unique set of values of K and M_s. To do this, we will apply the grid search method which, following the discussion in section 4.2.2, will now be based on generating a large number of 'reference' magnetization curves for a dense set of different, systematically varying, values of K and M_s and comparing individually each of such magnetization curves with the full set of generated curves. If uniqueness holds, then every magnetization curve will match ideally only itself, if not, there will be a set of different values for the parameters that will match one magnetization curves. In practice each loop contains errors due to the thermal noise. These errors propagate into the output of the inverse problem. Because of this, instead of having a unique match between a set of data and the 'reference' table, there is a range of parameters that describe well the magnetisation curve. In this case the uniqueness is define as χ^2 having just one minimal value. If there are more minimum values of χ^2, then the the uniqueness is not satisfied.

We computed magnetization curves for particle distributions with packing fractions 0.1, 0.2, 0.3, 0.4, and for the non-interacting case (packing fraction 0.0). The overall

shape of the sample was taken to be a sphere, i.e. $c/a = 1$, and the temperature range chosen from 10K to 185K consistently with experiments. We generated a grid with K between $2 \cdot 10^4$ erg/cm^3 and $5 \cdot 10^5$ erg/cm^3 in steps of $2 \cdot 10^4 erg/cm^3$ and M_s between 80 emu/cm^3 and 560 emu/cm^3 in in steps of 20 emu/cm^3.

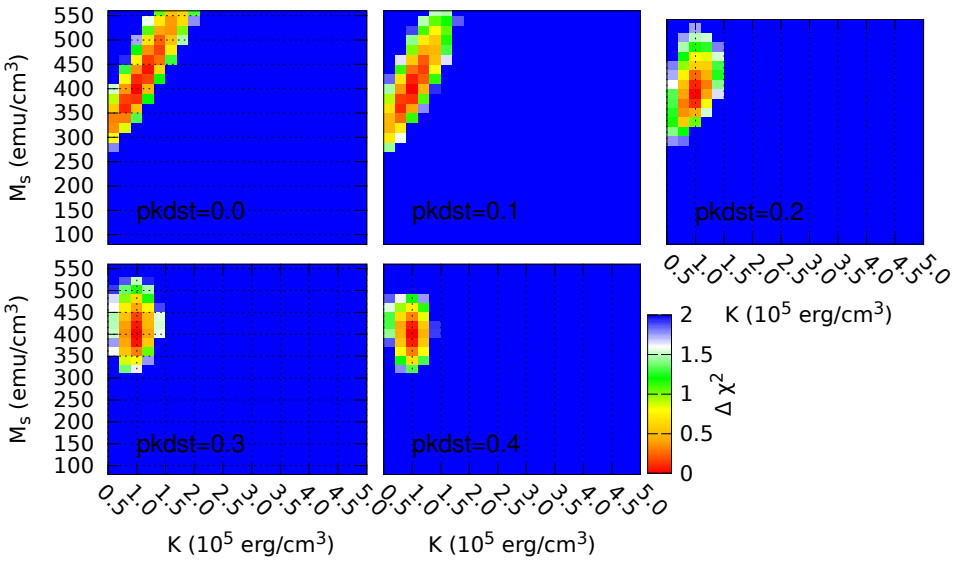

Figure 6.3: $\Delta\chi^2_{norm}$ map for 99% confidence interval for finding K=$1.0 \cdot 10^5$erg/cm^3 and $M_s = 400$emu/cm^3 at 20K and different packing fractions. For all the packing fractions (from 0.0 to 0.4) the optimum parameters are K = $1.0 \cdot 10^5$erg/cm^3 and M_s= 400 emu/cm^3. The parameter correlations changes from a positive correlation, for packing fraction 0.0, to an uncorrelated case for packing fraction of 0.4.

Figure 6.3 shows the resulting $\Delta\chi^2_{norm}$ maps obtained by comparing the input magnetization curve data set for $K = 1 \cdot 10^5$erg/cm^3, $M_s = 400$ emu/cm^3, $T = 10$K to the reference function tables for different particle packing fractions. In all the cases there exist an optimum solution within the chosen M_s and K range and the chosen 50% statistical confidence level. The size and shape of the contour depends on the packing fraction, which represents the developing $M_s - K$ parameter correlation. In the non-interacting case (0 packing fraction), the correlation is linear. This means that, with the 99% statistical confidence, the reference functions with a specific ratio of K and M_s match the input function. In other words, if this ratio is preserved the magnetization curves in that parameter range are indistinguishable. For larger packing fractions

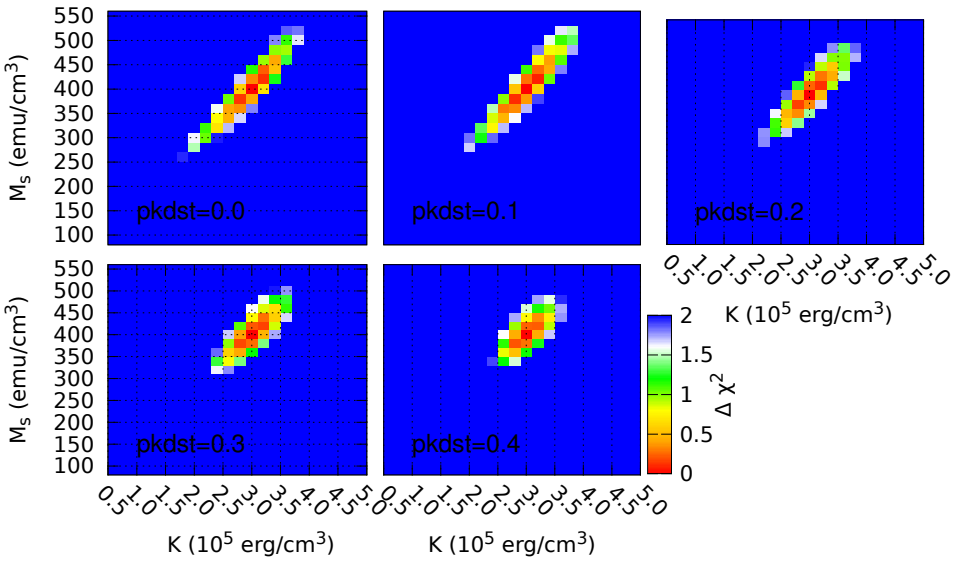

Figure 6.4: $\Delta\chi^2_{norm}$ map for 99% confidence interval for finding K=3.0 $\cdot 10^5$erg/cm^3 and $M_s = 400$emu/cm^3 at 20K and different packing fractions. For all the packing fractions (from 0.0 to 0.4) the optimum parameters are obtained correctly. The parameters are positive correlated, for all the packing fraction, but the errors of the optimum parameters are decreasing with increasing packing fraction.

the inter-particle interactions become stronger and the 'good match' elliptical contour rotates towards the horizontal orientation. Also the contour shrinks towards the circular shape suggesting a convergence of the errors towards a unique value of M_s and K. This effect of interactions depends on the balance between thermal energy, interaction energy and anisotropy energy. If we consider a large anisotropy (figure 6.4) the effect of interactions on $M_s - K$ parameter correlation is reduced. If we compare figure 6.4 and 6.3 we can see that for small packing fraction, meaning weak interaction, there is no difference between solving the inverse problem for K = $1 \cdot 10^5$ erg/cm^3 and for K = $3 \cdot 10^5$ erg/cm^3. For larger interaction there is an evident difference. For large K the errors decrease as for low K, but have different values. Also for large K, the ellipsoidal contour of the $\Delta\chi^2$ does not change the orientation as in low K case. With increasing temperature the interactions become less important and correlations are less visible. We can see from figure 6.5 the 2D map for $\Delta\chi^2_{norm}$ at 160K. The main aspect of the graph is that K is not well defined. The contour plot of the errors covers the entire range

of anisotropy values. This can be explain by the fact that with higher temperature the superparamagnetic behaviour is dominant and this does not depend on anisotropy.

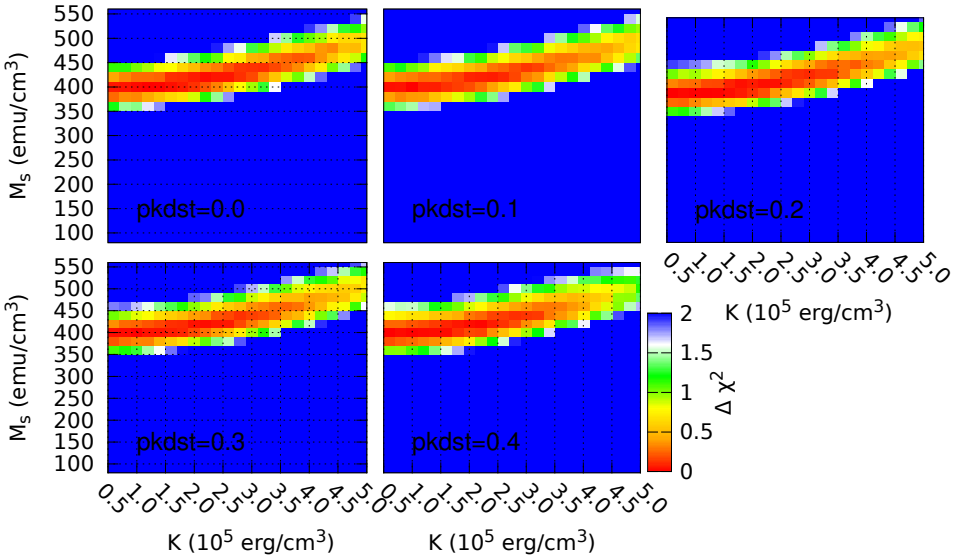

Figure 6.5: $\Delta\chi^2_{norm}$ map for 99% confidence interval for finding K=$1.0 \cdot 10^5$erg/cm^3 and $M_s = 400$emu/cm^3 at 160K and different packing fractions. For all the packing fractions (from 0.0 to 0.4) the optimum parameters are obtained correctly, but the errors for K are too large for the result to be meaningful.

For all temperatures and all packing fractions the above system has just one solution for K and M_s and it corresponds to the right solution. Next we focus on the error in determining the solution. As disused in section 4.2, the errors of the obtained parameters are important. If we analyse figure 6.5, it can be argued that the uniqueness of the solution is not satisfied. The magnetization curve for K=$1 \cdot 10^5$ erg/cm^3, $M_s = 400$ emu/cm^3 at 160K is described by any value of anisotropy in the range we investigated. There is just one minimal value of χ^2. The uniqueness is satisfied but the errors for K are very large. For this reason the results are not meaningful or not well defined. As suggested in section 4.2 the uniqueness of the inverse problem must be justified by relative small errors of the results. How small the errors need to be for the result to be meaningful depends on the aim of the investigation. We want to identify the value of parameters (in this case K and M_s) as good as possible. For this reason we investigate a broad range of temperatures. M_s is well defined for all temperature and interaction

strengths but for K the error-bars at higher temperature are too large for the result to be meaningful. In conclusion for low temperature we can use the inverse problem to obtain K and M_s, but for high temperature just M_s can be calculated.

To illustrate how relevant the shape of the sample is, we present a situation in which the effect is very strong: a thin film system with the same properties as the system presented before, except for the shape of the sample. For strong interactions we consider the field perpendicular to the thin film plane. Figure 6.6 illustrates the $\Delta\chi^2_{norm}$ 2D map at 10K for c/a=0.0 and the rest of parameters are as in the previous example. It can be seen that the correlation between K and M_s is more strongly dependent on interactions. This also influence the errors. Thus, the interactions play a very important role in finding the right solution. If the interactions in the model are not consistent with the sample we want to investigate, then it is unlikely we will be successful in identifying the parameters correctly.

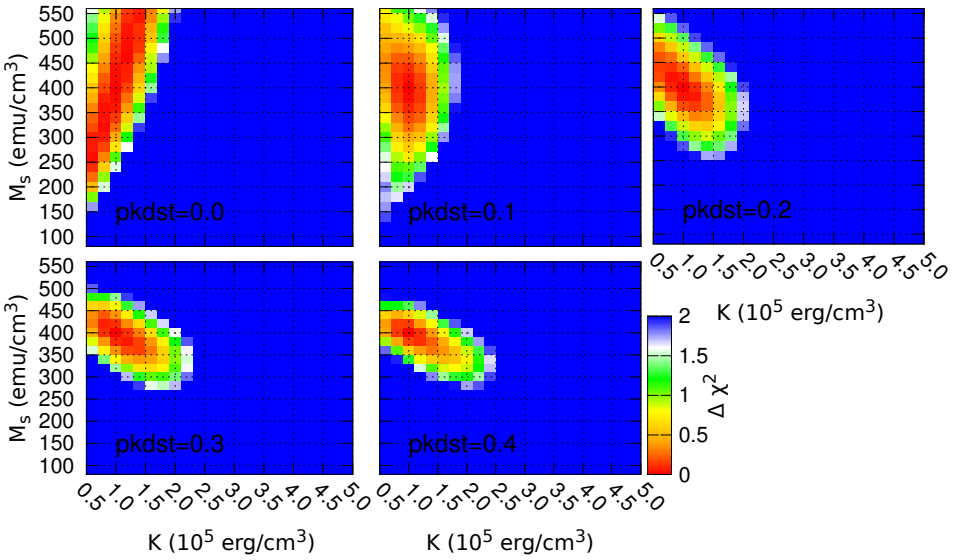

Figure 6.6: $\Delta\chi^2_{norm}$ map for 99% confidence interval for finding K=$1.0 \cdot 10^5$erg/cm^3 and $M_s = 400$emu/cm^3 at 10K and different packing fractions. c/a=0.0 and the field is applied out of the plane of the sample. The parameter correlations are strongly affected by the packing fractions. For the non-interacting system (packing fraction equal to 0.0) the parameter correlation is positive, at packing fraction 0.1 the parameters are uncorrelated and for larger packing fraction the parameters are negative correlated.

6.4 Identification of the properties of experimental samples

In this section we apply the methodologies developed above to study the experimental data presented in section 6.1. In this case, the applicability of our approaches depends on how accurately the Monte-Carlo model can be used as a reference to capture the relevant physics. If the model is realistic, then the identified model parameters will be accurate and the overall identification supported by high quality fits. On the other hand, if the model fails to be realistic, then systematic deviations from the expected (actual) physical parameters emerge, even though the fits can still be of high quality. Such behaviour has not been found in the previous section because both the input and reference functions were based on the same model.

Following the discussion in the previous section we begin by considering the identification of M_s and K from the experimental data. It is expected, that K will be quantifiable accurately only at low temperatures. To apply the grid search method, we consider samples of various geometries, and take log-normal particle size distribution with mean diameter equal to $dm = 6.7$ nm and standard deviation σ_{dm} =15% as TEM measurements suggest. We generate our system with a packing fraction of 0.33 consistent with the experiment. Then we compute reference magnetization curves for a dense mesh of K and M_s values as specified in the previous section.

First we investigate a second sample with the same properties as the sample described in section 6.1. The only exception consist in the demagnetisation factor c/a, which we estimated to be 0.16. The grid search method for this case yielded K in a rather broad range $4 \cdot 10^4 - 5 \cdot 10^5$ erg/cm^3, which is to be expected based on the uniqueness study given in the previous section. The identified values of M_s have been found increasing with temperature from about 200 emu/cm^3 to 400 emu/cm^3 as shown in Figure 6.7. The fit results show that there is a temperature region around 100K-150K where a rather sharp transition in M_s occurs. This transition behaviour is unexpected, and it is not clear at the moment whether this is physical or an artefact in the modelling. The most straightforward test is to check the effect of demagnetising field factor by changing the c/a. We can do this by analysing the sample shown in figure 6.1 in section 6.1, for which we simply set $c/a = 1$. The final results are qualitatively similar -

although the identified magnetisation saturation limits now extend from 200 emu/cm^3 to 500 emu/cm^3, the transition behaviour is again observed in the similar temperature range. We have also confirmed the transition by applying the Levenberg-Marquardt algorithm where c/a has been included as a fit parameters, which gave $c/a \approx 1$ and the values of M_s in the range from 200 emu/cm^3 to 500 emu/cm^3 where the upper limit is now close to the expected value for Fe_3O_4 (magnetite, 450 emu/cm^3). This thus demonstrates that although changing the demagnetising field contribution by tuning the c/a ratio results in quantitative adjustments in the observed trends, qualitatively the transition behaviour seems to be present in all cases.

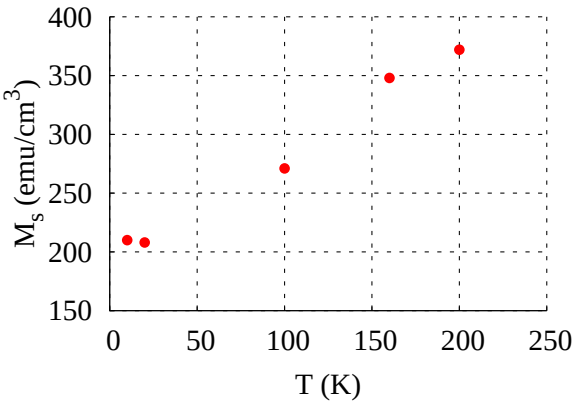

Figure 6.7: M_s values obtain solving the inverse problem for different temperature. The results are presented for a second sample with the same properties as the sample described in section 6.1, but with c/a equal to 0.16. The saturation magnetisation increases with temperature from 210 emu/cm^3 at 10K to 370 emu/cm^3 at 200K.

The above results indicate that interactions are too strong and just changing the demagnetizing field is not sufficient. The fact that the interactions are strong becomes apparent at lower temperatures where the model does not compensate well for the observed behaviour which results in the suppressed M_s from the inverse problem investigation. The packing fraction has been chosen consistently with the experimental observations and therefore we want to keep it. An alternative way to control the packing fraction and thus the interaction strength is by tuning the magnetic volume of particles. Although the TEM analysis suggests that the particle size is on average 6.7 nm the actual magnetic volume might be smaller. In the following we will focus only on the first sample shown in figure 6.1, where we have more temperature points and

thus more robust data. To model this we consider that the particles have a core-shell structure in which the magnetic core represents a part of the total size of particle as viewed from the TEM image. For this we generate a system of particles with a mean diameter of 6.7 nm and standard deviation of 15%, with packing fraction of 0.33. Then we allow the particles' magnetic core to vary but maintaining the total size as initially generated. The magnetic core will have the same distribution of size. The shape of the real sample is not well defined and so the c/a ratio will be also a fit parameter to optimise the effect of the sample's shape. In a first approximation we consider a fixed value of M_s equal to 450 emu/cm^3, a value close to the bulk one. The unknown parameters, K, dm and c/a are the ones needed to be obtained from solving the inverse problem. For calculating χ^2 we consider constant σ as discussed in section 5.2, and consider 50% confidence for determining the goodness of the fit and 99% confidence interval for estimating the errors.

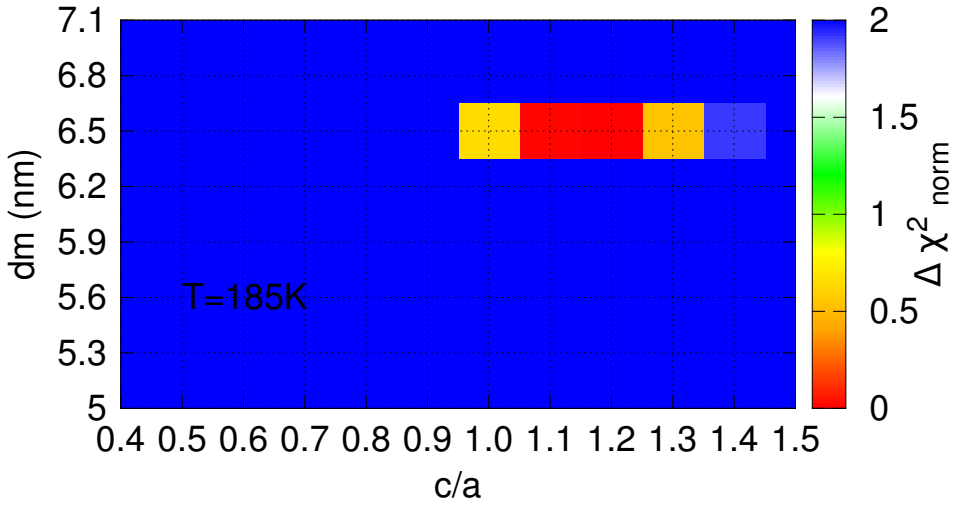

Figure 6.8: Grid search method results for dm and c/a for experimental data with $M_s = 450$emu/cm^3 and $\sigma_{dm} = 15\%$ at 185K. The optimum particle size is 6.5 nm and the ratio c/a is in the interval [0.95, 1.45].

To apply the grid search method for just two parameters we used the fact that at high temperature the anisotropy does not play an important role (as discussed in previous section and shown in figure 6.5). We first use the grid search method at the high temperature to obtain the optimal values of dm and c/a and then used the obtained values for c/a to find at low temperature K and dm. In figure 6.8 the results are presented for 185K. At 185K we investigated dm and c/a. The best value for c/a is 1.1 and 6.5 nm for the average size of the particle. Taking into account the errors at 99% confidence level the interval for c/a is [0.95, 1.45] and for dm the interval is [6.3 nm, 6.7 nm]. The investigation at lower temperature were done using c/a=1.0. In

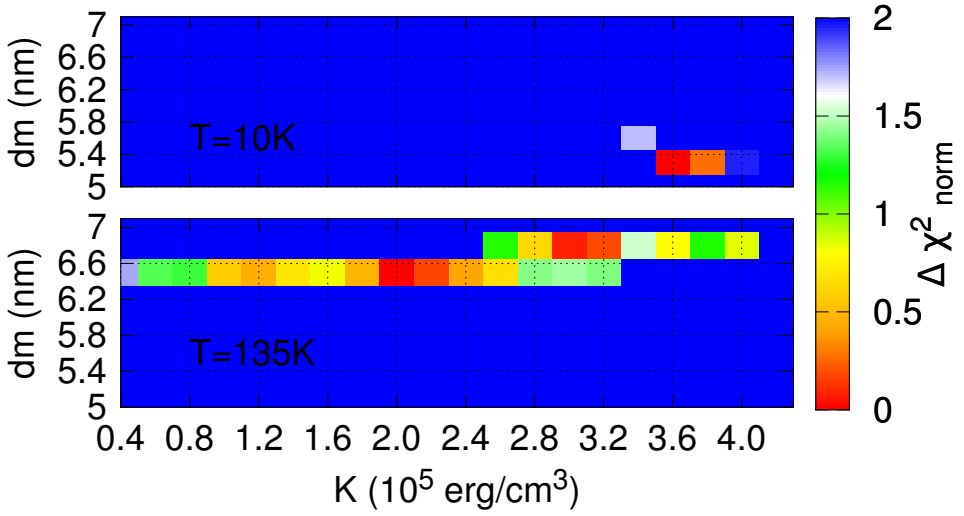

Figure 6.9: Grid search method results for dm and K for experimental data with $M_s =$ 450emu/cm^3 and $\sigma_{dm} = 15\%$ at 10K and 135K. The optimum size is 5.3 nm at 10K, whereas at 135K it is between 6.35 nm and 6.75 nm.

figure 6.9 the results for 10K and 110K can be seen. All the results are summarise in table 6.1. The optimal value of anisotropy is decreasing with increasing temperature, but the errors at high temperature are too large to have a clear trend. For the size of the magnetic core there is an increase from 5.3 nm at 10K to 6.5 nm at 185K with relatively large error bars at intermediary values of temperature. The difference between the size of particles obtained at low and high temperature is unexpected. To investigate this behaviour we analysed the approximation we used:

1. M_s equal to 450 emu/cm^3
2. σ_{dm} equal to 15%
3. The effect of the shape of the sample is approximated with the demagnetization factor from an ellipsoid of revolution

T (K)	$Dm_{\text{best fit}}$ (nm)	$Dm_{\max}$ (nm)	$Dm_{\min}$ (nm)	$K_{\text{best fit}}$ $(10^5 \cdot \text{emu/cm}^3)$	$K_{\max}$ $(10^5 \cdot \text{emu/cm}^3)$	$K_{\min}$ $(10^5 \cdot \text{emu/cm}^3)$
10	5.3	5.45	5.15	3.6	3.9	3.5
35	5.6	5.75	5.45	3.2	3.5	3.1
60	6.2	6.35	5.75	3.0	3.3	2.7
85	6.2	6.65	6.05	2.2	3.3	1.9
110	6.5	6.75	6.35	2.6	3.5	2.1
135	6.5	6.75	6.35	2.0	4.1	0.9

Table 6.1: Results from the grid search method containing the best value for dm and K. For 99% confidence level the range of the two parameters are included

The last consideration cannot be improved in the model because the shape of the experimental sample is not well defined, but the first two approximations can be addressed. We consider 5 discreet values of M_s between 380 and 460 emu/cm^3. For values under 380 emu/cm^3 there are no good solutions at high temperature for confidence levels as low as 50% and values bigger than 460 emu/cm^3 are not expected for magnetite. Considering multiple values for σ_{dm} increases the difficulty of obtaining the fit. If we change the value of σ_{dm} in an existing system, then it is possible that two neighbour particle to overlap. To avoid this, for each different σ_{dm}, a new system must be generated. This means that the LM method cannot be applied for finding the optimal σ_{dm}. The values used for σ_{dm} are $5\%, 10\%, 15\%, 20\%$ and 25%. The best results are obtained for σ_{dm} equal with 5% and M_s equal to 450 emu/cm^3. The results for K and dm for the two values for σ_{dm} are illustrated in figure 6.10. The K values are similar in the error limit for both results. For dm there is not a significant improvement if we look at the optimal value except for the 10K case where the new value is 5.6 nm in comparison with the previous one 5.3 nm, but if we consider also the error bars, there is a important difference. For $\sigma_{\text{dm}} = 15\%$ the difference in size between all the temperature is in the

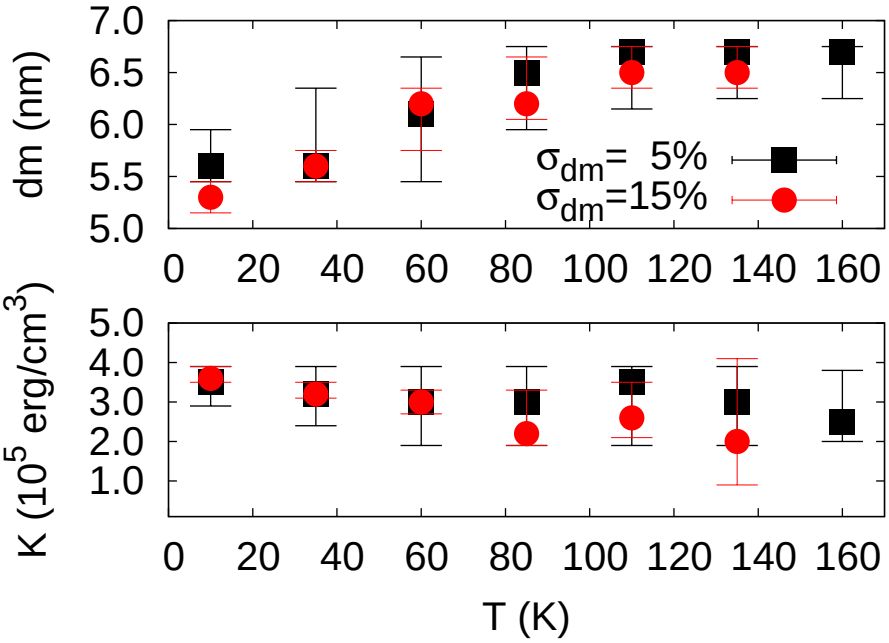

Figure 6.10: Grid search method results for K and dm with $\sigma_{dm} = 15\%$ (green dots) and 5% (red squares).

interval [0.8 nm, 1.6 nm] where as in the latter case, for $\sigma_{dm} = 5\%$ all the values of dm vary in the range [0.3 nm, 1.3 nm]. Overall a value of 6.1 nm $\pm$ 0.65 nm describes the experimental data for all temperatures.

We were expecting to obtain a unique value of dm for all temperature. The fact that the particle size at 10K and 185K do not overlap in the error limit raises the following questions: why this disagreement appears and is this real or just an artefact of the model. We saw in section 6.3, when we investigated the uniqueness of the inverse problem for our model, that the inverse problem has a unique solution. Therefore the two methods used for solving the inverse problem (Grid search method and Levenberg-Marquardt) are not the issue.

A possible reason may be due to a discrepancy between our Monte-Carlo model of the system and the actual real system. It could be that our model is not complex enough and a more detailed model is needed, but there is no clear evidence for this. A more plausible explanation is that the interaction from the model are not in good agreement with the experimental case. We saw in section 6.4 that changing the interaction strength by changing the packing fraction has a important influence on the parameter correlation and implicitly on errors. By trying to model experimental data with with a stronger interacting system, it may be that M_s or dm will be smaller at low temperature to compensate. At high temperature, because interaction are less important due to the large thermal noise, the disagreement between the model and real system is not reflected in the output of the inverse problem. In this case the result from high temperature probably describes the experimental data most accurately, and the low temperature results are an artefact.

Another possible explanation for the temperature dependence of the mean particle size with temperature can be due to a canted state, which has been seen in magnetic nanoparticles [49, 50]. The canted state decreases with temperature, that means that the effective magnetic core increases. In this case the variation of dm with temperature can occur to take this effect into account. A difference of maximum 1.3 nm between the values of M_s at 10K and at 185K corresponds to approximately 4 atomic layers. One to four atomic layers for the canting state is plausible but to validate this assumption more experimental measurement are required.

7

Conclusions and future work

In this thesis we studied the inverse problem of identifying properties of magnetic nanoparticle systems from magnetisation versus field curves. For this we developed a realistic Monte-Carlo model of 3D particle systems containing spherical nanoparticles with uniaxial anisotropy (section 4.1.4). Log-normal distribution of size and anisotropy values were considered with spherical distribution of easy axis. Magnetostatic interaction and thermal effects were taken into account. This allowed to calculate magnetisation curves at different temperatures, which were then validated against the known analytical results in section 5.1. Sections 4.2 and 5.2 where dedicated to studying the inverse problem.

For the inverse problem we concentrated on two different approaches: Levenberg-Marquardt algorithm and Grid search method. The grid search method has advantage in that it offers information about the uniqueness of the solution and the model parameters correlation, but it becomes inefficient for evaluating more than 2 model parameters. The Levenberg-Marquardt approach is an optimal algorithm for obtaining the solutions from fitting to many parameters but when implemented on its own it does not provide detailed information about the uniqueness of solutions beyond the errorbar calculation.

The methodologies presented in the thesis are of broad applicability and can be implemented to include any physical parameter relevant to nanoparticle system. In this thesis we focus on studying the inverse problem for identifying anisotropy (K) and saturation magnetisation (M_S). As discussed in chapter 6, both parameters can be accurately obtained at low temperature, but at large temperature just M_S can be calcu-

lated with this approach. In the high temperature region, superparamagnetic behavior dominates and the exact value of anisotropy is less important. In the last chapter we applied the developed methods to investigate a set of experimental measurements, obtained for systems of spherical magnetite nanoparticles at different temperatures from 10K to 185K.

The methodologies developed in this thesis provides a good insight into the properties of the experimental samples and suggests a possible sound interpretation of the measurement results. Moreover, the value of this study consists also in that it demonstrates the difficulties in the interpretation of experimental results obtained from complex nanoparticle systems. Addressing the questions of uniqueness is essential to avoid drawing erroneous conclusions about the nature of the experimental samples.

7.1 Future outlook

The straightforward continuation of the present work is to extend the present analysis to understand the question of uniqueness with respect to additional parameters, such as different choices of particle anisotropy or volume distributions, different types of particle arrangements ranging from random spatial distributions to highly uniform lattices. A question of fundamental nature is to understand the reasons for the observed non-uniqueness of inverse problems on microscopic basis. This involves linking the macroscopic observation of parameters correlation with microscopy investigation of domain formation and particle correlation. The method can be also used to study the inverse problem for other parameters such as particle size and its distribution, anisotropy and its distributions.

Another research direction anticipated in the future is to improve the methodologies developed in this thesis by incorporating different solutions types for addressing the inverse problem. The present study was based on identification using magnetisation curves and we found that identification of the anisotropy parameter K was non-unique in the high temperature range. Better results might have been obtained by including also minor hysteresis in the analysis or by concentrating on data of a different nature such as the temperature dependent magnetization data, or the magnetization relaxation data. It is also possible that combination of several different solutions might be nec-

essary to achieve fully unique identification of model parameters. These questions are highly nontrivial and give prospects for long-term future work.

Appendix A: Least squares fitting. General notions

When analysing a real phenomenon there is a necessity to have a theoretical model of that phenomenon and experimental evidence of the model so that it can be rigorously investigated and used to make prediction. In general an experiment consists in investigation of a system response to variation of different parameters. From the theoretical point of view this is described by a set of equations or in general by a mathematical model that explains the physical phenomenon involved.

A large group of experiments consist in investigation of the response of the system to the variation of different parameters. This results are summarised numerically in two groups: independent variables (those variables that are controlled by experimentalist) and dependent variables (values that characterise the response of the system to the independent variable). In general x is used to describe the independent variable and y for the dependent variable and for each x corresponds a value y. In the case of magnetization curves the magnetic response of the system is measured as a function of the applied field.

To gain a better understanding of the investigated phenomenon a model is used. A model consists of a set of mathematical equations that describe the main feature of the behaviour of the system as function of the independent variables. A way to obtain more information from experimental data is to fit those data to a function, f(x), that describe the phenomenon. Function f(x) has also a set of coefficients. The reason to fit the function to the data is to find all or a part of the coefficients. They are called fitting parameters or parameters of interest (**p**) and their values need to be obtained

whereas the rest of the coefficients are known (from the model or from other experiment). Overall our function depends on the independent variable x and fit-parameters ($\mathbf{p}$):

$$y = f(x, \mathbf{p}) \tag{1}$$

The large use of this methodology has made the fitting algorithms an important subject in mathematics and in physics. Although they have been studied for a long time a general rigorous method does not exist. The fitting results will describe the system with a certain probability. Based on that probability and on the approach used, the idea of a good or bad fit is defined. All the methods have a set of elements that needs to be included:

1. First a meaningful model that describes the data is chosen. Choosing an appropriate model is very important. For example you can fit almost any set of data with a high-order polynomial function but the result is not meaningful because it does not describe the physics of the investigated phenomenon.

2. Then a function called figure-of-merit function that calculate the agreement between data and the model is selected [40]. This function differs from algorithm to algorithm.

3. The extreme point (in general the minimum) of the above function with respect to the parameters ($\mathbf{p}$) corresponds to the best-fit values of the parameters ($\mathbf{p}_{fit}$). This transforms the algorithm into a minimisation problem.

4. The values for best-fit parameters are determined.

5. The errors of the obtained parameters are evaluated. The experimental data are not perfect, they will contain errors. For this reason there will not be just a simple set of parameters that will describe the data. Repeating the experiment several times will give slightly different points that will have different best-fit parameters. Depending on the model and on the errors in the experiment, the best-fit parameters could have the errors too large to be useful.

6. The goodness-of-the-fit is evaluated. This is also very important because even if we obtain the fit parameters with acceptable errors the results may not describe the data well enough. This can happen for different reasons:

   (a) The model is not good or incomplete;

   (b) The errors are too big;

   (c) There is one or more extra parameters that are needed to be taken into account;

   (d) The function has more than one minimum. This makes the minimisation problem difficult;

The first element is not relevant for a general description of the fitting algorithm. For this section we can assume a good model with general form like:

$$y = f(x, \mathbf{p}) \tag{2}$$

There are a large number of methods for fitting and also different ways to test if the fit is meaningful or not. The most used methods are based on minimisation of squared errors between the experimental data and prediction values from mathematical models. This methods are called least squares and the main element of these methods, that are used in this thesis are presented in the next paragraphs [40]. Assuming that the measurement errors are independent and randomly distributed around the 'true' value as a Gaussian distribution, then the probability that a point is around the mean or expected value (the 'true' value) has the following form:

$$P_i = Ce^{-\frac{1}{2}\left(\frac{y_i-\overline{y_i}}{\sigma_i}\right)^2}\Delta y \tag{3}$$

where y_i is the experimental data corresponding to the independent value x_i, $\overline{y_i}$ is the mean value for the same x_i, σ_i is the standard deviation of y_i and C is a constant. This assumption is valid for the magnetization measurement, because the dominating source of noise are the thermal fluctuations which give a Gaussian distribution of errors. We want to find parameters for the function $f(x, \mathbf{p})$ that describe $\overline{y_i}$. Replacing $\overline{y_i}$ with the

function $f(x_i, \mathbf{p})$, the probability will be big if $f(x, \mathbf{p})$ and $\overline{y_i}$ are very close and will decrease if they are further away.

$$P_i = Ce^{-\frac{1}{2}\left(\frac{y_i - f(x_i, \mathbf{p})}{\sigma_i}\right)^2} \Delta y \tag{4}$$

For all the points the total probability will be the product of each of the above probabilities:

$$P_i = C^N \prod_{i=1}^{N} e^{-\frac{1}{2}\left(\frac{y_i - f(x_i, \mathbf{p})}{\sigma_i}\right)^2} \Delta y \tag{5}$$

$$= C^N e^{-\frac{1}{2}\sum_{i=1}^{N}\left(\frac{y_i - f(x_i, \mathbf{p})}{\sigma_i}\right)^2} \Delta y \tag{6}$$

The best set of parameters will correspond to the highest probability P. Maximising P is equivalent to minimising the sum from exponent, called chi-square:

$$\chi^2 = \sum_{i=1}^{N} \left(\frac{y_i - f(x_i, \mathbf{p})}{\sigma_i}\right)^2 \tag{7}$$

Now we have a figure-of-merit function, $\chi^2(\mathbf{p})$ and we need to find the minimum of the function relative to parameters $\mathbf{p}$. Depending on the method, this step can be simple or complex. For the grid search method this is done very fast, just calculating $\chi^2(\mathbf{p})$ for each simulated loop and $\mathbf{p}_{fit}$ corresponds to the smallest $\chi^2(\mathbf{p})$. The second method (Levenberg-Marquardt method) is more complex because from a set of "guess" parameters, the algorithm automatically in a optimal way searches through parameter space for the smallest $\chi^2(\mathbf{p})$ corresponding to the best-fit parameter. If the data that are fitted are perfect (not affected by noise) or the model is perfect (there is just one possible output form the model), then the best fit will correspond to $\chi^2(\mathbf{p}) = 0.0$ and parameters, $\mathbf{p}$, will be exactly calculated. This is the ideal case, but the magnetization measurements are affected by different errors and also the theoretical model takes into account thermal fluctuation. In this case the errors will propagate to $\chi^2(\mathbf{p})$ and therefore $\chi^2(\mathbf{p})_{min} > 0.0$ and $\mathbf{p}_{fit}$ will be determined with an error. First of all we need a way to evaluate how small $\chi^2(\mathbf{p})_{min}$ should be to find out if the fit is meaningful or not. If

the experiment is repeated the new set of data will be slightly different and also $\chi^2(\mathbf{p})$ will be different. Under the assumption of Gaussian errors the obtained $\chi^2(\mathbf{p})$ value has a probability of having any value. Because χ^2 is a sum of Gaussian distributed terms, $\chi^2(\mathbf{p})_{min}$ follows a chi-square distribution with N_p-M_f degrees of freedom, where N_p is the number of data points and M_f is the number of fitted parameters:

$$Q(\chi^2, v) = \frac{1}{2^{v/2}\Gamma(v/2)}\chi^{v/2-1}e^{-x/2} \quad \text{where v=}N_d\text{-}M_f \tag{8}$$

There is a certain probability ($Q_{\chi^2>\chi^2_{lim}}$) that the obtained $\chi^2(\mathbf{p})_{min}$ is smaller that χ^2_{lim} due to chance:

$$Q_{\chi^2>\chi^2_{lim}} = \int_{\chi^2_{lim}}^{\infty} Q(\chi^2, v)dx \tag{9}$$

Once the goodness of the fit is analysed, we can proceed to evaluate the errors in estimating the fitting parameters. The errors are determined by investigating how fast χ^2 is changing from the minimum values with the change in parameters from the best fit values. For this the difference between the chi-square of a set of parameters and the minimum chi-square is calculated. The difference of the two has the notation $\Delta\chi^2$ and is following a chi-square distribution with M degrees of freedom. To evaluate the errors with a given confidence (1-Q), $\Delta\chi^2$ has a limit value which corresponds to a contour region in parameters space. This contour region corresponds to the errors of the fit-parameters. The probability Q and $\Delta\chi^2_{lim}$ have the same definition as for determining the goodness of the fit. Although χ^2 and $\Delta\chi^2$ have the same definition, they are two different element:

1. Value of χ^2 at minimum: a measure of goodness of fit. The degrees of freedom are equal to the difference between the number of data to be fitted and the number of parameters to be fitted.

2. How quickly χ^2 changes as a function of the parameter ($\Delta\chi^2$): a measure of the uncertainty on the parameter. The degrees of freedom are equal to the number of fitted parameters.

References

[1] Q. A. Pankhurst, J. Connolly, S. K. Jones, and J. Dobson, "Applications of magnetic nanoparticles in biomedicine," *Journal of Physics D: Applied Physics*, vol. 36, pp. R167–R181, July 2003. 1

[2] S. Laurent, D. Forge, M. Port, A. Roch, C. Robic, L. Vander Elst, and R. N. Muller, "Magnetic iron oxide nanoparticles: synthesis, stabilization, vectorization, physicochemical characterizations, and biological applications.," *Chemical reviews*, vol. 108, pp. 2064–110, June 2008. 1

[3] M. Colombo, S. Carregal-Romero, M. F. Casula, L. Gutiérrez, M. P. Morales, I. B. Böhm, J. T. Heverhagen, D. Prosperi, and W. J. Parak, "Biological applications of magnetic nanoparticles.," *Chemical Society reviews*, vol. 41, pp. 4306–34, June 2012. 1

[4] A. Stancu, C. Pike, L. Stoleriu, P. Postolache, and D. Cimpoesu, "Micromagnetic and Preisach analysis of the First Order Reversal Curves (FORC) diagram," *Journal of Applied Physics*, vol. 93, no. 10, p. 6620, 2003. 2

[5] A. P. Chen, R. Egli, and B. M. Moskowitz, "First-order reversal curve (FORC) diagrams of natural and cultured biogenic magnetic particles," *Journal of Geophysical Research*, vol. 112, p. B08S90, Aug. 2007. 2

[6] O. Hovorka, Y. Liu, K. Dahmen, and a. Berger, "On the ability to determine intrinsic switching field distributions from hysteresis loops in the partially correlated magnetization reversal regime," *Journal of Magnetism and Magnetic Materials*, vol. 322, pp. 459–468, Feb. 2010. 2

[7] O. Hovorka, R. F. L. Evans, R. W. Chantrell, Y. Liu, K. a. Dahmen, and A. Berger, "Validation of ΔH(M,ΔM)-technique for identification of switching field distributions in the presence of thermal relaxation," *Journal of Applied Physics*, vol. 108, no. 12, p. 123901, 2010. 2

[8] R. Chantrell, J. Popplewell, and S. Charles, "Measurements of particle size distribution parameters in ferrofluids," *IEEE Transactions on Magnetics*, vol. 14, pp. 975–977, Sept. 1978. 2

[9] R. Chantrell, N. Walmsley, J. Gore, and M. Maylin, "Calculations of the susceptibility of interacting superparamagnetic particles," *Physical Review B*, vol. 63, p. 024410, Dec. 2000. 2, 38

[10] H. Gavin, "The Levenberg-Marquardt method for nonlinear least squares curve-fitting problems," *Environmental Engineering*, pp. 1–15, 2011. 2

[11] K. Nogi, M. Hosokawa, M. Naito, and T. Yokoyama, *Nanoparticle Technology Handbook*. Elsevier, 2012. 3

[12] O. Ozdemir and D. Dunlop, "Low-temperature properties of a single crystal of magnetite oriented along principal magnetic axes," *Earth and planetary science letters*, vol. 165, pp. 229–239, 1999. 3

[13] a.G. Roca, J. Marco, M. Morales, and C. Serna, "Effect of Nature and Particle Size on Properties of Uniform Magnetite and Maghemite Nanoparticles," *Journal of Physical Chemistry C*, vol. 111, pp. 18577–18584, Dec. 2007. 3

[14] a. G. Roca, M. P. Morales, K. O'Grady, and C. J. Serna, "Structural and magnetic properties of uniform magnetite nanoparticles prepared by high temperature decomposition of organic precursors," *Nanotechnology*, vol. 17, pp. 2783–2788, June 2006. 3

[15] G. F. Goya, T. S. Berquo, F. C. Fonseca, and M. P. Morales, "Static and dynamic magnetic properties of spherical magnetite nanoparticles," *Journal of Applied Physics*, vol. 94, no. 5, p. 3520, 2003. 3

[16] N. Pérez, P. Guardia, a. G. Roca, M. P. Morales, C. J. Serna, O. Iglesias, F. Bartolomé, L. M. García, X. Batlle, and a. Labarta, "Surface anisotropy broadening of the energy barrier distribution in magnetic nanoparticles.," *Nanotechnology*, vol. 19, p. 475704, Nov. 2008. 3

[17] K. Buschow and F. de Boer, *Physics of magnetism and magnetic materials*. Springer, 2003. 5

[18] B. Cullity, *Introduction to magnetic materials*. Wiley-IEEE Press, 2011. 10

[19] R. Skomski, *Simple models of magnetism*. Oxford University Press, 2008. 10, 11

[20] J. Osborn, "Demagnetizing factors of the general ellipsoid," *Physical Review*, no. h 8, 1945. 14

[21] E. Stoner and E. Wohlfarth, "A mechanism of magnetic hysteresis in heterogeneous alloys," *Philosophical Transactions of the Royal Society of London. Series A, Mathematical and Physical Sciences*, vol. 240, no. 826, pp. 599–642, 1948. 16

[22] A. Stancu, *Magnetization processes in particulate ferromagnetic media*. Cartea Universitară, 1996. 17

[23] H. Pfeiffer, "Determination of anisotropy field distribution in particle assemblies taking into account thermal fluctuations," *physica status solidi (a)*, vol. 118, no. 1, pp. 295–306, 1990. 23

[24] D. Weller and M. F. Doerner, "Extremely high-density longitudinal magnetic recording media," *Annual Review of Materials Research*, vol. 30, pp. 611–644, 2000. 24

[25] D. Weller, "Thermal effect limits in ultrahigh-density magnetic recording," *Magnetics, IEEE Transactions on*, vol. 35, no. 6, pp. 4423–4439, 1999. 24

[26] L. Néel, "Some theoretical aspects of rock-magnetism," *Advances in Physics*, vol. 4, no. 14, pp. 191–243, 1955. 24

[27] W. F. Brown, "Thermal Fluctuations of a Single-Domain Particle," *Physical Review*, vol. 130, no. 5, pp. 1677–1686, 1963. 25

[28] N. Metropolis, A. Rosenbluth, and M. Rosenbluth, "Equation of state calculations by fast computing machines," *The journal of chemical*, vol. 21, no. 3, pp. 1088–1092, 1953. 26, 27

[29] E. D. Biasi, C. Ramos, and R. Zysler, "Metropolis algorithm for simulating hysteresis in ferromagnetic nanoparticles," *Physica B: Condensed*, vol. 372, pp. 345–349, 2006. 26

[30] J. Garcıa-Otero, M. Porto, and J. Rivas, "Monte Carlo simulation of hysteresis loops of single-domain particles with cubic anisotropy and their temperature dependence," *Journal of magnetism and*, vol. 203, pp. 268–270, 1999. 26

[31] M. El-Hilo, R. Chantrell, and K. O'Grady, "A model of interaction effects in granular magnetic solids," *Journal of applied physics*, vol. 84, no. 9, pp. 5114–5122, 1998. 26, 35

[32] U. Nowak, R. Chantrell, and E. Kennedy, "Monte Carlo simulation with time step quantification in terms of Langevin dynamics," *Physical review letters*, vol. 84, no. 1, pp. 163–166, 2000. 29

[33] O. Chubykalo, J. Kauffman, B. Lengsfield, and R. Smirnov-Rueda, "Long-time calculation of the thermal magnetization reversal using Metropolis Monte Carlo," *Journal of Magnetism and Magnetic Materials*, vol. 242, pp. 1052–1056, Apr. 2002. 29

[34] O. Chubykalo, U. Nowak, R. Smirnov-Rueda, M. Wongsam, R. W. Chantrell, and J. Gonzalez, "Monte Carlo technique with a quantified time step: Application to the motion of magnetic moments," *Physical Review B*, vol. 67, Feb. 2003. 29

[35] X. Cheng, M. Jalil, H. Lee, and Y. Okabe, "Mapping the Monte Carlo scheme to Langevin dynamics: a Fokker-Planck approach," *Physical review letters*, vol. 96, no. 6, p. 067208, 2006. 29

[36] H. Pfeiffer, "Influence of thermal fluctuations on the magnetic properties of particle assemblies," *physica status solidi (a)*, vol. 122, no. 1, pp. 377–389, 1990. 31

[37] H. K. Lee, T. C. Schulthess, D. P. Landau, G. Brown, J. P. Pierce, Z. Gai, G. a. Farnan, and J. Shen, "Monte Carlo simulations of interacting magnetic nanoparticles," *Journal of Applied Physics*, vol. 91, no. 10, p. 6926, 2002. 35

[38] D. Cimpoesu, L. Spinu, and A. Stancu, "The state dependence of the dynamic interactions in nanostructured particulate systems," *Journal of Applied Physics*, vol. 97, no. 10, p. 10J501, 2005. 35

[39] J. Coey, *Magnetism and Magnetic Materials*. Magnetism and Magnetic Materials, Cambridge University Press, 2010. 36

[40] W. H. Press, B. P. Flannery, S. A. Teukolsky, and W. T. Vetterling, *Numerical Recipes in Fortran: The Art of Scientific Computing*. Cambridge University Press, 2 ed., Sept. 1992. 41, 85, 86

[41] P. J. Flanders and M. P. Sharrock, "An analysis of time-dependent magnetization and coercivity and of their relationship to print-through in recording tapes," *Journal of Applied Physics*, vol. 62, no. 7, p. 2918, 1987. 54

[42] R. Chantrell, G. Coverdale, and K. O'Grady, "Time dependence and rate dependence of the coercivity of particulate recording media," *Journal of Physics D:*, vol. 1469, pp. 26–29, 1988. 54, 55

[43] O. Hovorka, R. Evans, and R. Chantrell, "Rate-dependence of the switching field distribution in nanoscale granular magnetic materials," *Applied Physics Letters*, vol. 97, no. 6, p. 062504, 2010. 54

[44] M. Bahiana, J. Pereira Nunes, D. Altbir, P. Vargas, and M. Knobel, "Ordering effects of the dipolar interaction in lattices of small magnetic particles," *Journal of Magnetism and Magnetic Materials*, vol. 281, pp. 372–377, Oct. 2004. 67

[45] D. Kechrakos and K. Trohidou, "Magnetic properties of dipolar interacting single-domain particles," *Physical Review B*, vol. 58, pp. 12169–12177, Nov. 1998. 67

[46] M. Fähnle and H. Kronmüller, "The influence of spatially random magnetostatic, magnetocrystalline, magnetostrictive and exchange fluctuations on the law of approach to ferromagnetic saturation of amorphous ferromagnets," *Journal of Magnetism and Magnetic Materials*, vol. 8, pp. 149–156, 1978. 67

[47] R. Grossinger, "A critical examination of the law of approach to saturation," *Phys. Status Solid*, vol. 665, no. I, 1981. 67

[48] M. Celasco and P. Mazzetti, "Saturation approach law for grain-oriented polycrystalline magnetic materials," *Magnetics, IEEE Transactions on*, pp. 372–378, 1969. 67

[49] M. Darbandi, F. Stromberg, J. Landers, N. Reckers, B. Sanyal, W. Keune, and H. Wende, "Nanoscale size effect on surface spin canting in iron oxide nanoparticles synthesized by the microemulsion method," *Journal of Physics D: Applied Physics*, vol. 45, p. 195001, May 2012. 80

[50] K. L. Krycka, R. a. Booth, C. R. Hogg, Y. Ijiri, J. a. Borchers, W. C. Chen, S. M. Watson, M. Laver, T. R. Gentile, L. R. Dedon, S. Harris, J. J. Rhyne, and S. a. Majetich, "Core-Shell Magnetic Morphology of Structurally Uniform Magnetite Nanoparticles," *Physical Review Letters*, vol. 104, p. 207203, May 2010. 80